Supplement of Earth Syst. Sci. Data, 13, 3927–3950, 2021
https://doi.org/10.5194/essd-13-3927-2021-supplement

Open Access Earth System Science Data

Supplement of

The global forest above-ground biomass pool for 2010 estimated from high-resolution satellite observations

Maurizio Santoro et al.

Correspondence to: Maurizio Santoro (santoro@gamma-rs.ch)

Supplement of manuscript

The global forest above-ground biomass pool for 2010 estimated from high-resolution satellite observations

Maurizio Santoro et al.

S.1 Auxiliary datasets

The European Space Agency (ESA) Climate Change Initiative Land Cover (CCI-LC) dataset consists of annual (1992-2018) maps classifying the world's land cover into 22 classes (Table S6). The overall accuracy of the 2010 land cover dataset was 76% (Defourny et al., 2014), with the most relevant commission and omission errors in mixed classes or in regions of strongly heterogeneous land cover. The land cover maps were provided in equiangular projection with a pixel size of 0.00278888° in both latitude and longitude. In this study, we used the land cover map of 2010, version 2.07. The dataset was re-projected to the map geometry of our AGB dataset.

The Global Ecological Zones (GEZ) dataset produced by the Food and Agriculture Organization (FAO, 2001) divides the land surface into 20 zones (Figure S2, Table S2) with "broad yet relatively homogeneous natural vegetation formations, similar (but not necessarily identical) in physiognomy" (FAO, 2001). In this study, the dataset has been rasterized to the geometry of the images requiring stratification by ecological zones.

Spatially explicit datasets of GSV representative of dense forests were obtained to support the model calibration described in Sections S.2 and S.3. This dataset was first compiled by assigning a value to the centre of each tile in a regular 2°×2° grid. Where available, *in situ* measurements from field plots or spatially explicit datasets of GSV were used. The GSV of dense forests was then defined as the 90th percentile of the histogram within the 2°×2° area (Santoro et al., 2011). Elsewhere, it was estimated with an empirical piece-wise linear function (Santoro et al., 2015a) starting from values of the average biomass reported at provincial or national level. For tiles including several provinces or nations, the average biomass representative for the tile was obtained by weighting the individual averages by the area

of each within the tile. In regions where values based on inventory measurements were unavailable but we could gather more than one map of AGB (preferably based on laser scanning observations), we estimated the biomass of dense forest as the joint 90th percentile of the histogram of the map values. For areas lacking any form of biomass estimates, the IIASA FAO 0.5° dataset of global biomass (Kindermann et al., 2008) was used. The value for the biomass of dense forests was then set equal to the maximum of the 16 values within the 2°×2° tile. Figure S15 shows the origin of the biomass values used to compute the biomass of dense forests. If the reference data expressed biomass as AGB, we divided the AGB by the wood density and the Biomass Expansion Factor (BEF) described in Section S.5.

The procedure used to characterize the GSV of dense forests globally was quite crude and should be considered a first-order approximation. Attaching a single value to areas covering thousands of km^2 is unlikely to be sufficient to characterize it in regions with several types of vegetation. We assumed that the spatial variability of the maximum biomass would be small, but this assumption fails in regions with transitions between ecosystems (e.g., tropical forest and savannah). Errors and uncertainties propagating from the input datasets, the rules implemented to estimate the biomass of dense forests from the data available in a given tile, and the BCEF values could not be avoided.

We tried to reduce some of the weaknesses in the dataset by taking into account that the maximum biomass reached by forests across different ecoregions is expected to depend on natural factors such as temperature, precipitation or disturbance regime, as well as on anthropogenic factors such as varying types of forest management. For this, we computed the averages for nineteen WorldClim bioclimatic variables and for the ICESat GLAS observations of canopy density and height in each 2° × 2° grid cell (DUE GlobBiomass - Algorithm Theoretical Basis Document). The models were developed at the level of FAO ecoregions using the initial estimates of the dense forests GSV in our database as response and the WorldClim and ICESat GLAS layers as predictors. Once calibrated, the models were then used to predict the GSV of dense forests globally at a resolution of 0.2° × 0.2° (Figure S16). For an assessment of this dataset, refer to (DUE GlobBiomass - Algorithm Theoretical Basis Document).

S.2 BIOMASAR-C implementation

To estimate the coefficient β, we gathered a number of spatially explicit maps of GSV and simulated canopy density, η, with Eq. (S3) by varying β within a range of realistic values from 0.004 to 0.014 m^{-1}.

The exponential in Eq. (S1) represents two-way tree transmissivity, where α is the two-way tree attenuation (unit: dB/m) and h is the tree height.

$$e^{-\beta V} = 1 - \eta(1 - e^{-\alpha h}) \quad \text{(S1)}$$

We finally associated to each of the FAO ecozones the value of β minimizing the difference between modelled canopy density and the MODIS Vegetation Continuous Fields (VCF) canopy density estimates (DUE GlobBiomass - Algorithm Theoretical Basis Document). As a result, β varied between 0.012 m^{-1} in tropical rainforest and 0.004 m^{-1} in arid environments. In general, higher values were associated with ecozones with closed canopy forests (DUE GlobBiomass - Algorithm Theoretical Basis Document). Although such an approach entails a substantial amount of uncertainty, it was found to be the only practical way to assess the spatial variability of the coefficient β given the lack of large-scale datasets of *in situ* observations. Note that seasonal conditions could not be accounted for with this approach.

To estimate σ^0_{gr} and σ^0_{veg}, we applied the procedure described in (Santoro et al., 2015, 2011). For a given pixel, the parameter σ^0_{gr} corresponded to the median value of measured backscatter for pixels characterized by a canopy cover below a given threshold. A mask derived from the CCI Land Cover dataset was used to exclude pixels with 0% canopy density belonging to classes not related to vegetation (water bodies, permanent snow and ice, bare soil and urban areas). Here, canopy cover was represented by the MODIS VCF data product of 2010, which was averaged and resampled to the geometry of the ASAR data (DUE GlobBiomass - Algorithm Theoretical Basis Document). The estimation procedure used a moving window approach, in which the size of the estimation window and the threshold were adapted in space (Santoro et al., 2011). The same approach was applied to derive an estimate of the backscatter of dense forests, σ^0_{df}, i.e., the median measured backscatter for pixels characterized by a canopy cover above a given threshold (Santoro et al., 2011). Since the parameters σ^0_{veg} express the backscatter for a theoretically completely opaque vegetation layer, the estimate of σ^0_{veg} was obtained by correcting the measurement for dense forests for the residual contribution from the ground through canopy gaps.

$$\sigma^0_{veg} = \frac{\sigma^0_{df} - \sigma^0_{gr} e^{-\beta V_{df}}}{1 - e^{-\beta V_{df}}} \quad \text{(S2)}$$

In Eq. (S2), V_{df} represents the GSV of dense forests (Section S.1).

S.3 BIOMASAR-L implementation

To estimate the model parameter β, we fitted the model in Eq. (S1) to measurements of canopy density and height at ICESat GLAS footprints and corresponding estimates of GSV from various sets of maps (NACP Aboveground Biomass and Carbon Baseline Data (NBCD 2000); Rodríguez-Veiga et al., 2019). The two-way tree attenuation α was assumed to be 0.5 dB m^{-1} (see below for details). The model fitting was stratified by the FAO Global Ecological zones (DUE GlobBiomass - Algorithm Theoretical Basis Document). Low values for β of ~0.004-0.005 m^{-1} provided the closest fit to the predictors in the boreal and sub-tropical dry ecozone. In temperate and sub-tropical humid forest regions, higher values in the range of 0.006-0.008 m^{-1} were obtained whereas in the wet tropics the model fit closest to the predictors was obtained with 0.011 m^{-1}. A global look-up table was then generated relating ecological zones and estimated β.

The estimation of σ^0_{gr} and σ^0_{df} follows the same procedure as in BIOMASAR-C although with a slightly different implementation in terms of thresholds of canopy density. The ALOS PALSAR backscatter mosaic in a 1° x 1° tile is divided into individual dates and each date is then divided into 15 x 15 km^2 blocks. The canopy density threshold used to delineate areas of low canopy density is increased from 0% in steps of 1% until the required number of pixels with low canopy density (100 pixels) is found. The maximum allowed canopy density threshold is set to 20%. The canopy density threshold used to delineate dense forest is reduced in steps of 1% from 100% until the required number of pixels (100) with a canopy density above the selected threshold is found. The minimum threshold is set to 70%. If this requirement cannot be fulfilled, a direct estimate of the respective parameter is not considered possible and interpolations based on adjacent areas with valid estimates of the model parameters is required. Interpolation is primarily required in areas of continuous dense forest cover, such as the Amazon and Congo basins, where the number of pixels corresponding to sparse forest cover is limited. The 30 m Landsat-based tree canopy cover data product of 2010 (Hansen et al., 2013) resampled to the geometry of the ALOS PALSAR dataset was used to delineate areas of low and high canopy density. The model parameters σ^0_{gr} and σ^0_{df} were then set equal to the mode of the backscatter distribution in areas of low and high canopy density, respectively. For the latter, a kernel-smoothing algorithm to the histogram of high canopy backscatter was applied to avoid spurious effects on the estimation of the mode.

For L-band, the model proposed to estimate σ^0_{veg} in Eq. (S2) had to account for the non-negligible tree attenuation. It was therefore rewritten from the original formulation of the Water Cloud Model with gaps (Askne et al., 1997):

$$\sigma^0_{veg} = \frac{\sigma^0_{df} - \sigma^0_{gr} T_{df}}{1 - T_{df}} \quad \text{(S3)}$$

where Tdf represents the forest transmissivity of the densest forests in the area of interest, which itself is considered a function of residual canopy gap fraction, η_{df}, and canopy height, h_{df}:

$$T_{df} = \left(1 - \eta_{df}\right) + \eta_{df} e^{-\alpha h_{df}} \quad \text{(S4)}$$

The residual transmissivity, T_{df}, was estimated from the LiDAR-based estimates of canopy height and density for footprints covering forests with a canopy density larger than 90% according to the Landsat tree cover dataset. Significant effects on the estimates of σ^0_{veg} were only observed for values of α well below 0.5 dB m^{-1} which, based on our current understanding, may be associated with images acquired under frozen conditions. The L-band data used to generate the mosaics were primarily acquired under unfrozen conditions so that the use of a fixed value for α of 0.5 dB/m appeared justified.

S.4 Merging of GSV estimates

The derivation of the weights is outlined below; refer to (DUE GlobBiomass - Algorithm Theoretical Basis Document) for illustrations and interpretation of the individual weights.

Since the forest transmissivity term $e^{-\beta V}$ represents the sensitivity of the SAR backscatter to GSV, the weight that reflects the difference in sensitivity between C- and L-band was defined as the difference in the derivatives of the forest transmissivity term, $e^{-\beta V}$,

$$w_s = \left|\frac{\partial T_L}{\partial V}\right| - \left|\frac{\partial T_C}{\partial V}\right| \quad \text{(S5)}$$

The transmissivity at L- and C-band, T_L and T_C, used the ecoregion-specific values for β at each frequency. The BIOMASAR-C GSV map was assumed to act as a reference because of the reliable spatial distribution of GSV compared to other maps (DUE GlobBiomass - Algorithm Theoretical Basis Document). As the performance of the BIOMASAR algorithm improves when the retrieval relies on a large number of backscatter observations, this weight was refined by also accounting for the number of observations available at L- and C-band (N_L and N_C, respectively).

$$w_s = \left|\frac{\partial T_L}{\partial V}\sqrt{N_L}\right| - \left|\frac{\partial T_C}{\partial V}\sqrt{N_C}\right| \quad \text{(S6)}$$

This weight can then be rescaled to the range 0 to 1 to obtain normalized weights:

$$w_{s,norm} = \frac{(w_s - min(w_s))}{max(w_s - min(w_s))} \quad \text{(S7)}$$

The weighting scheme that accounts for local errors in the model training and inversion was based on a comparison between the transmissivity simulated with either the BIOMASAR-C+ or the BIOMASAR-L GSV (first term in Eq. (S1)) and the transmissivity simulated with the aid of globally available canopy density (Hansen et al., 2013) and height (Simard et al., 2011) maps (second term in Eq. (S1)). For the latter, we assumed a two-way tree attenuation of 0.5 dB/m for L- and 2 dB/m for C-band. Although errors in the optical canopy density and forest height maps used to simulate the transmissivity might have influenced the simulations, we took the fact that one of the GSV maps was less consistent with the assumed relationship between transmissivity and GSV as indication that, locally, the more consistent map should have been preferred, i.e., should have been given more weight.

The weighting scheme was formalized by (i) simulating the transmissivity at C- and L-band, $T_{sim(C)}$ and $T_{sim(L)}$, using the global maps of canopy density and height with the second term in Eq. (S3), (ii) fitting the first term of Eq. (S1) first to the simulated C-band transmissivity $T_{sim(C)}$ and BIOMASAR-C+ GSV and then to the simulated L-band transmissivity $T_{sim(L)}$ and BIOMASAR-L GSV, and (iii) generating a modelled set of transmissivity at C- and L-band with the corresponding model fits, $T_{mod(C)}$ and $T_{mod(L)}$. The model fitting procedure was applied on a per ecoregion basis. Weights were created by evaluating at pixel level for which map (i.e., BIOMASAR-C+ or BIOMASAR-L) the difference between T_{sim} and T_{mod} was smaller:

$$w_t = |T_{sim}(C) - T_{mod}(C)| - |T_{sim}(L) - T_{mod}(L)| \quad \text{(S8)}$$

and normalizing w_t to the range 0 to 1 for each ecoregion separately:

$$w_{t,norm} = \frac{(w_t - \min(w_t))}{max(w_t - \min(w_t))} \quad \text{(S9)}$$

By definition, this weight was high where the BIOMASAR-L map was more consistent with the underlying forest transmissivity.

The weighting scheme to account for the poorer characterization of the distortions due to topography on the backscatter in the ALOS PALSAR mosaics was based on the layer of local incidence angles provided with the mosaics. Since it was assumed that radiometric terrain effects in the mosaics were primarily due to inaccurate estimates of the pixel scattering area (Ulander, 1996; Small, 2011), which scales approximately with the inverse of the sine of the incidence angle, the definition of the weights was based on the difference in pixel scattering area between flat terrain (38° incidence angle) and the pixel area estimated from the local incidence angle.

$$\Delta_{area} = 100 \cdot |1 - \sin(38°)| / \sin(\theta_i) \quad \text{(S10)}$$

The weight, w_{topo}, for the BIOMASAR-L map was then defined by linearly scaling Δ_{area} between 0 to 1 with 1 representing flat terrain (38° incidence angle) and 0 reflecting Δ_{area} values beyond 30%.

The three weights were finally combined by assuming that w_s and w_t are equally important whereas w_{topo} should lower the proportion of the BIOMASAR-L GSV estimate to the integrated estimate over steep terrain. The weight applied to the BIOMASAR-L GSV estimates was therefore defined as:

$$w_L = 0.5 \cdot \left(w_{s,norm} + w_{t,norm}\right) \cdot w_{topo,norm} \quad \text{(S11)}$$

Accordingly, the weight applied to the BIOMASAR-C+ estimates was:

$$w_C = 1 - w_L \quad \text{(S12)}$$

S.5 Conversion from GSV to AGB

S.5.1 Data

The *in situ* wood density (WD) datasets originated from the Biomass And Allometry Database (BAAD) (Falster et al., 2015), TRY (Kattge et al., 2011), TRY gap-filled (Schrodt et al., 2015), Phillips et al. (Phillips et al., 2003) and Schepaschenko et al. (Schepaschenko et al., 2017) databases (Figure S17). For the Biomass Expansion Factor (BEF), we explored the BAAD (Falster et al., 2015), Agriculture, Forestry and Other Land Use (AFOLU, ftp://mars.jrc.ec.europa.eu/Afoludata/Public/all_datasets.html) and Schepaschenko et al. (Schepaschenko et al., 2017) databases (Figure S18). The characterization of environmental conditions that stand as the independent covariates for predicting WD and BEF was supported by data extracted from global databases of climatological (Fick and Hijmans, 2017), atmospheric (Wilson and Jetz, 2016) and soil properties (Batjes et al., n.d.). In addition, we included in the set of potential covariates land surface properties such as vegetation indices (e.g. NDVI (Pinzon and Tucker, 2014), EVI (Huete et al., 2002), FPAR (Myneni et al., 2002), productivity (Tramontana et al., 2016), vegetation cover (Sexton et al., 2013), height (Simard et al., 2011) and land cover (Defourny et al., 2014). These variables may embed information on the development stage of forests, and as such on spatial variability of resource allocation strategies, which influence the spatial distribution of WD and BEF. For these variables we further computed a number of statistics: (i) annual means, standard deviations on spatial variability computed for the datasets with finer spatial resolution; and (ii) temporal trends, standard deviation and percentiles estimated for temporally varying datasets.

S.5.2 Methods for WD estimation

We used Random Forests (RF) to predict WD given its ability to generalize and extract nonlinear relationships between target and predictor variables (Breiman, 2001) and its wide use in ecology and biogeochemistry (Tramontana et al., 2016). RF emerged as the most robust method among a wide set of machine learning approaches in predicting the spatial patterns of plant traits using remote sensing observations and climatological data (Moreno-Martínez et al., 2018). Given the high number of potential covariates for predicting WD, we conducted two variable importance analyses: (1) evaluation of variable

importance based on permutation tests for each variable (Moreno-Martínez et al., 2018) and (2) a feature selection algorithm (Jung and Zscheischler, 2013). These analyses were performed to predict WD in two distinct ways.

A) Tree/plot scale

The set of covariates were extracted for every valid record of wood density, yielding a total of approximately 435 potential predictors. The final set of covariates for prediction was determined based on the feature selection approach (Jung and Zscheischler, 2013) which supports the construction of the final model. The procedure was executed and repeated four times to include a two-factor experiment: (1) including or removing the gap-filled records in the TRY database and (2) including classification information about leaf type and leaf phenology (Table S9, models 4 to 7). These experiments aimed at assessing the prediction sensitivity to (1) data representativeness, given that the wood density data in these global databases included few observations in Oceania and Africa, and few in the Americas, except for the gap-filled TRY; and (2) to acknowledge the strong variations in WD within Plant Functional Types (PFT) (Thurner et al., 2014).

B) Landscape scale

The landscape level WD is estimated as $WD_j = \sum_{i=1}^{N} WD_i \cdot f_{j,i}$, where the WD in a given grid-cell j (WD_j) is estimated as the weighted average of all the WD values representing the abundance of different PFTs (Table S6) (i) in that same grid-cell j ($f_{j,i}$) (Moreno-Martínez et al., 2018). Given the dependence on MODIS vegetation indexes, each grid-cell has a 500 m × 500 m spatial resolution. Grid-cells were selected based on a high resolution land cover map (30m resolution), for which a WD_j is computed based on *in situ* observations not separated by more than 100 km from the corresponding MODIS pixel and if more than 50% of the PFT composition was represented by nearby WD observations (Moreno-Martínez et al., 2018). Here we also performed the experiment of including/excluding the TRY gap-filled records. Overall, this resulted in a dataset for training with 5,000 data points (grid-cells) for the gap-filled example (Table S9, model 1) and 4,000 data points (grid-cells) for the non-gap-filled dataset (Table S9, model 3). The prediction of WD also relied on an alternative gap filling (Moreno-Martínez et al., 2018) (Table S9, model 2).

Similarly to other modelling ensemble studies, we also explored the behaviour of a weighted average of individual wood density estimates by using for each FAO Global Ecological zone the method-specific biases and variances as weights.

$$WD = \left(\frac{\sum_{i=1}^{7} \frac{1}{bias_i} WD_i}{\sum_{i=1}^{7} \frac{1}{bias_i}} + \frac{\sum_{i=1}^{7} \frac{1}{\mathrm{var}_i} WD_i}{\sum_{i=1}^{7} \frac{1}{\mathrm{var}_i}} \right) \times 0.5 \quad \text{(S13)}$$

Both the landscape level estimates as well as the tree/plot level results show unbiased estimates of WD and explained 60% and 70% of variance in cross-validation for tree/plot and landscape level estimates, respectively (Figure S19). The variability in landscape level wood density was significantly explained using the WorldClim set of bioclimatic variables and MODIS Normalized Difference Vegetation Index (NDVI) and Enhanced Vegetation Index (EVI) as covariates (Figure S19). In addition, leaf properties and phenology information substantially improved the performance of the RF results in cross-validation for tree/plot level estimates, explaining about 60% of the variance in the observations when not including gap-filled data in the training set. Part of the limitation in tree/plot estimates stemmed from (i) the fact that several observations may share locations, implying that different plot-level estimates have exactly the same input covariates (categorical and climatological), and (ii) a representation mismatch between local conditions and coarse covariates. Comparing the normalized root mean square errors (NRMSE) between WD observations and predictions through a progressive aggregation of WD records showed a substantial improvement already at aggregation of 10 records (Figure S19, bottom), suggesting a higher reliability in the predictions at coarser scales. This is further confirmed by comparing the global WD predictions at locations of *in situ* observations (Figure S20) aggregated per FAO Global Ecological Zone (Table S2) or bioclimatic class (Table S10).

To understand whether the spread of estimated and observed WD as in Figure S19 and Figure S20 could be explained by different capabilities of a specific model to predict wood density in different environmental conditions, we compared the Pearson's correlation coefficient, the RMSE and the estimation bias per FAO ecozone and for each WD prediction model. The statistical analysis was constrained to include only observed wood densities based on at least 10 samples per location (Figure

S21). No single model appeared to perform better across all ecozones. Furthermore, the lower correlations and higher biases found within ecozones (Figure S19) in comparison to across ecozones (Figure S20) reflect a poorer performance of any model locally, which can result from: (i) lower variability in model predictions than in observations because of natural variability; (ii) lower variability in the environmental variables that are less variable within an ecozone, which could result in lower variance in predictions; (iii) higher impact of the spatial scale mismatch between observed wood density and covariates included in the machine learning models; (iv) a limited, and unbalanced observational datasets across ecozones. Regarding the last aspect, to the best of our knowledge, the database of wood density observations was the largest ever used for such kind of predictions; still, the lack of observations in large parts of the globe and/or ecological zones may cause models to generate different, and poorer, predictions regionally.

The wood density map obtained with the plot-based predictions approach using the gap-filled TRY database (model 5 in Figure S21) seemed to have overall the most robust performance (even if it did not perform the best within ecological zones) followed by the landscape model using gap-filled data (model 1 in Figure S21). However, the former model appeared to be negatively biased across the wet tropics and to miss the broad longitudinal pattern in the Amazon basin (Chave et al., 2009, 2014). We explain the lack of accuracy as a consequence of the paucity of wood density observations in these regions. In contrast, the latter model returned almost unbiased estimates, and appeared to reproduce documented spatial patterns of WD across the tropics.

We therefore analysed the result of integrating the predictions from the landscape-based approach for FAO Global Ecological Zones representative of wet and moist tropics into the plot-based dataset of WD using the gap-filled TRY database (Figure S22, right hand-side). The integrated WD dataset reproduced the major patterns of wood density. The lowest values were obtained across the boreal zone of evergreen conifers; slightly higher values corresponded to the region dominated by deciduous conifers. The temperate forests of northwest US and Europe exhibited further slightly higher wood densities. In the tropics, dry forests exhibited higher wood densities than wet forests.

Observed and predicted wood densities (Figure S22, panels on the right hand-side) presented reasonable agreement; however, the predictions could explain only 25% and 38% of the observed variability of wood density. Still, the integrated dataset of wood density was of higher quality when compared to the

weighted average of the estimates from the individual model (Figure S22, panel on the left hand-side). Averaging reduced the uncertainties of the individual predictions but did not yield statistical improvement and reduced the variance of the predictions, which became substantially smaller than the variance of the observations. In addition, systematic differences between models in areas that were poorly or not represented in the wood density database hampered the determination of a robust bias term in Eq. (S13) and could propagate an unidentifiable uncertainty, or potentially regional bias, to the final estimates of wood density.

While the integrated WD dataset appeared to be the most reliable among all predictions obtained in this study, these results highlight the difficulties in grasping the controls of local variability of wood density with currently available datasets as a result of limitations in availability of *in situ* data and the mismatch in spatial representativeness of local factors controlling the variations in wood density.

S.6 Biomass reference data

We gathered datasets of plot inventory measurements, resulting in a total of 190,402 AGB observations. To assess our estimates, we retained AGB observations for plots (i) with precise coordinates (4-6 decimals for coordinates in decimal degrees), (ii) including trees with DBH ≥ 10 cm and (iii) at least 0.04 ha large and (iv) with a census date in or after the year 2000 to ensure temporal consistency with the 2010 epoch**.** In addition, we excluded double counts and plots that were deforested between the year of the included census and 2010 using the tree loss layer of the Global Forest Change data product as reference (Hansen et al., 2013). The database of plot inventory measurements of AGB consisted of 110,897 data values (Tables S2 and S3). Possible spatial mismatches between map pixels and forest plots may still result as a difference in the support size (resolution) and due to geolocation errors in both the remote sensing and the plot data.

For Russia, data for the Forest Managements Units (FMU) were available from the State Forest Register (SFR - http://goslesreestr.ru:7001/ForesterFO/). The median size of the FMUs is 116 kha. Although the SFR data refers to the year 2014, the actual forest inventory was accomplished over a wide range of years. About 50% of Russian forests were inventoried 25 or more years ago, especially in remote areas with low productivity forest. The actual forest area for the year 2010 was updated based on remote

354 sensing (Schepaschenko et al., 2015), while we assumed that the average biomass is unlikely to have
355 changed significantly in recent years and disturbances are compensated by increments.
356
357 GSV or AGB statistics were computed for Canada, United States, Mexico and Russia. Values reported in
358 the literature were gathered for 27 European countries, Chile, China, Japan, South Korea, Tanzania and
359 Mozambique. To avoid the per-unit average biomass derived from our estimates of biomass including
360 values in non-forest areas, our GSV and AGB maps were masked with the forest/non-forest mask derived
361 from the CCI Land Cover dataset of 2010.
362
363

Table S1. Total AGB estimated from global AGB datasets. In brackets is the total AGB in forests using the CCI Land Cover dataset as reference.

Reference	Year	Spatial resolution	Total AGB (Pg)
Pan et al. (Pan et al., 2011)	2007	inventory data	571 (n/a)
Kindermann et al. (Kindermann et al., 2008)	2005	0.5°	1,152 (555)
Hu et al. (Hu et al., 2016)	2004	0.01°	614 (562)
Liu et al. (Liu et al., 2015)	2010	0.25°	803 (569)
GEO-CARBON (Santoro et al., 2015; Avitabile et al., 2016a)	2000-2010	0.01°	454 (426)

Table S2. Legend of the FAO Global Ecological Zones dataset (FAO, 2001)

Domain	Global Ecological Zone (GEZ)		
	Code	Name	Code
Tropical	TAr	Tropical rain forest	11
	TAwa	Tropical moist deciduous forest	12
	TAwb	Tropical dry forest	13
	TBSh	Tropical shrubland	14
	TBWh	Tropical desert	15
	TM	Tropical mountain systems	16
Subtropical	SCf	Subtropical humid forest	21
	SCs	Subtropical dry forest	22
	SBSh	Subtropical steppe	23
	SBWh	Subtropical desert	24
	SM	Subtropical mountain systems	25
Temperate	TeDo	Temperate oceanic forest	31
	TeDc	Temperate continental forest	32
	TeBSk	Temperate steppe	33
	TeBWk	Temperate desert	34
	TeM	Temperate mountain systems	35
Boreal	Ba	Boreal coniferous forest	41
	Bb	Boreal tundra woodland	42
	BM	Boreal mountain systems	43
Polar	P	Polar	50

Table S3. Number of inventory plots per continent, average plot size, and census years.

Continent	Number of plots	Average plot size ± SD (ha)	Census year (range)
Europe	84,162	0.16 ± 0.08	2000-2014
Africa	3,106	0.22 ± 0.18	2004-2016
Asia	5,794	0.07 ± 0.36	2003-2012
Australia	9,113	0.13 ± 0.30	2000-2015
North America	4,047	0.04 ± 0.01	2000-2014
Mexico	4,045	0.16 ± 0	2006
South America	630	0.28 ± 0.22	2001-2015

Table S4. Metadata of ground reference datasets of AGB. DBH indicates diameter at breast height; WD indicates wood density, HGT indicates tree height.

ID	Continent	Country / Location	Extent	Vegetation type(s)	Year(s)	N. plots	Plot area (ha)	Min. DBH (cm)	Allometric equation	Parameters of allometric equation	Reference
AFR2	Africa	Sierra Leone / Gola	Local	Forest	2005-2007	593	0.08 - 0.125	10	(Chave et al., 2005) Moist	DBH, WD, HGT	(Lindsell and Klop, 2013)
AFR4	Africa	Ethiopia / Kafa	Local	Forest - Woodland	2011-2013	110	0.126	5	(Chave et al., 2005) Wet	DBH, WD	(DeVries et al., 2012)
AFR5	Africa	Ghana / Ankasa, Bia Boin, Dadieso	Local	Forest	2012-2013	71	0.05 - 0.16	5 / 10	(Chave et al., 2005) Moist	DBH, WD, HGT	(Vaglio Laurin et al., 2014; Pirotti et al., 2014)
AFR6	Africa	Tanzania / Eastern Arc Mountain	Local	Forest	2007-2010	24	0.08 - 1	10	(Chave et al., 2005) Moist	DBH, WD, HGT	(Willcock et al., 2014)
AFR7	Africa	DRC / Yangambi	Local	Forest (intact)	2011-2012	19	1	10	(Chave et al., 2005) Moist	DBH, WD, HGT	(Kearsley et al., 2013)
AFR8	Africa	Guinea-Bissau	National	Forest, Savanna, Mangrove	2007-2008	105	0.125	5	(Chave et al., 2005) Dry	DBH, WD, HGT	(Carreiras et al., 2012)
AFR9	Africa	Mozambique / Lugela	Local	Savanna	2011	41	0.126	5	(Ryan et al., 2011), (Chidumayo, 1997), (Chave et al., 2005) Dry, (Brown et al., 1989)	DBH, WD	(Carreiras et al., 2013)
AFR10	Africa	Cameroon	Local	Forest - Savanna	2007	18	0.5 - 1	10	(Chave et al., 2005) Dry / Moist	DBH, WD, HGT	(Mitchard et al., 2011)
AFR11	Africa	Uganda	National	Forest - Woodland - Savanna	2004-2005	726	0.25	3	(Drichi, 2003)	DBH, HGT	(Drichi, 2003; Avitabile et al., 2012)
AFR12	Africa	Uganda	Local	Forest	2008	108	0.16	10	(Chave et al., 2005) Dry / Moist	DBH, WD	(Avitabile et al., 2012)
AFR13	Africa	Uganda	Local	Forest	2008	25	0.5 - 1	10	(Chave et al., 2005) Moist	DBH, WD, HGT	(Mitchard et al., 2009)
AFR14	Africa	Mozambique	Local	Forest - Woodland	2006-2009	88	0.1 - 2.2	5	(Ryan et al., 2011)	DBH	(Ryan et al., 2012)
AFR15	Africa	Madagascar	National	Forest	2007-2013	680	0.13 / 0.28	5	(Chave et al., 2014)	DBH, WD, HGT	(Vieilledent et al., 2016)
AFR_FOS	Africa	Cameroon, DRC, Gabon, Ghana, Liberia	Local	Forest (intact)	2006-2016	144	0.25	10	(Chave et al., 2005) Moist	DBH, WD, HGT	(Schepaschenko et al., 2019)

AFR_GUB	Africa	Guinea Bissau	Local	Forest, woodland, Savanna	2007-2008	112	0.126	5	(Chave et al., 2005) Moist, (Komiyama et al., 2008) mangroves, (Pearson et al., 2007) palm trees	DBH, WD, HGT	(Carreiras et al., 2012)
AFR_KEN	Africa	Kenya	Local	Forest, Savannah, Mangrove	2014-2016	242	0.07	5	(Chave et al., 2014), (Muchiri and Muga, 2013) bamboos	DBH, WD, HGT	https://www.kefri.org/PDF/Publications/Kenya_FieldManual.pdf
SAM2	S. America	Brazil	National	Forest	2009-2015	281	0.09 - 1	5 / 10	(Chave et al., 2005) Moist	DBH, WD, HGT	(dos-Santos et al., 2019)
SAM3	S. America	Guyana	Local	Forest	2010-2011	111	0.126	5	(Chave et al., 2005) Moist	DBH, WD	(Brown et al., 2014)
SAM4	S. America	Peru / Madre de Dios	Local	Forest	2014	7	0.15	10	(Goodman et al., 2013) for palms, (Goodman et al., 2014)	DBH, WD, HGT	(Goodman et al., 2019)
SAM5	S. America	Brazil / Manaus	Local	Forest (secondary)	2014	23	0.6	5	(Chave et al., 2014), (Goodman et al., 2013) for palms	DBH, WD, HGT	n/a
SAM_FOS	S. America	Bolivia, Brazil, French Guiana, Guyana, Peru	Local	Forest (intact)	2001-2015	162	0.25 - 0.27	10	(Chave et al., 2005) Moist	DBH, WD, HGT	(Schepaschenko et al., 2019)
SAM_TAP	S. America	Brazil / Tapajos	Local	Forest (intact)	2009	46	0.25	10	(Brown et al., 1989)	DBH, HGT	(Da Conceição Bispo et al., 2012; Bispo et al., 2014)
CAM1	C. America	Mexico	National	Forest	2004-2008	4045	0.16	7.5	(Urquiza-Haas et al., 2007)	DBH, WD, HGT	(de Jong, 2013)
ASI1	Asia	Vietnam / Quang Nam	Province	Forest	2007-2009	2903	0.05	6	(Chave et al., 2005) Moist	DBH, WD, HGT	(Avitabile, 2014; Avitabile et al., 2016b)
ASI2	Asia	Laos / Xe Pian	Local	Forest	2011-2012	119	0.1 - 0.126	5	(Chave et al., 2005) Dry / Moist	DBH, WD	(WWF and ÖBf, 2013)
ASI3	Asia	Indonesia / Sabah	Local	Forest (concession)	2005-2008	92	0.5 - 1.5	10	(Chave et al., 2005) Moist	DBH, WD, HGT	(Morel et al., 2011)
ASI4	Asia	Indonesia / Riau	Local	Forest	2009-2010	70	0.015	5	(Komiyama et al., 2008), (Chave et al., 2005) Moist	DBH, WD	(Wijaya et al., 2015)
ASI5	Asia	India, China, Indonesia	Local	Forest (intact)	circa 2010	28	0.25 - 20	10	(Chave et al., 2005) Dry / Moist / Wet	DBH, WD, HGT	(Slik et al., 2013)
ASI8	Asia	Indonesia (Kalimantan)	Local	Mangrove	2008-2009	31	0.015	5	(Komiyama et al., 2008)	DBH, WD	(Murdiyarso et al., 2010)
ASI9	Asia	Vietnam / Quang Nam	Province	Forest	2011-2012	74	0.126	5	(Chave et al., 2005) Moist	DBH, WD, HGT	(Avitabile, 2014; Avitabile et al., 2016b)

ASI10	Asia	Philippines	National	Forest (and other types)	2003-2004	1210	0.5	10	(Chave et al., 2014)	DBH, WD, HGT	(Forest Management Bureau, 2010)
ASI11	Asia	China	Local	Forest	2000-2014	1267	0.1	2	Various methods (Zhang et al., 2019)	NA	(Zhang et al., 2019)
AUS1	Australia	Australia	National	Forest and shrublands	2000-2015	9113	0.005 - 25	0.3	(Paul et al., 2016)	DBH, WD, HGT	(TERN AusCover, 2016)
NAM1	N. America	Alaska	National	Forest	2005-2014	588	0.04	0	(Yarie et al., 2007)	DBH	(Liang et al., 2015)
NAM2	N. America	USA	Local	Forest	2000-2007	74	NA	0	NA	NA	
NAM3	N. America	Canada / Prince Edward Island	Province	Forest	2000-2014	591	0.01 - 0.04	0	(Ung et al., 2008)	DBH, HGT	n/a
NAM4	N. America	Canada / Nova Scotia	Province	Forest	2008-2012	2794	0.04	9	(Ung et al., 2008)	DBH, HGT	n/a
EU1	EU	Sweden	National	Forest	2007-2014	16819	0.015	NA	n/a	n/a	https://www.slu.se/en/Collaborative-Centres-and-Projects/the-swedish-national-forest-inventory/
EU2	EU	Spain	National	Forest	2000-2008	58185	0.196	7.5	Default biomass expansion factor (IPCC, 2006)	n/a	http://www.magrama.gob.es/es/desarrollo-rural/temas/politica-forestal/inventario-cartografia/inventario-forestal-nacional/
EU3	EU	The Netherlands	National	Forest	2012-2013	3021	5-20m radius	5	Default biomass expansion factor (IPCC, 2006)	n/a	(Schelhaas et al., 2014)
EU4	EU	Croatia	National	Forest	2006-2008	5967	0.004 - 0.126	0	(Cienciala et al., 2008), (Tabacchi et al., 2011)	DBH, HGT	n/a
EU_FOS	EU	Russia, Ukraine, Poland	Local	Forest	2014	170	0.27	2 / 5 / 7	n/a	n/a	(Schepaschenko et al., 2019)

Table S5. Summary of AGB datasets used for the inter-comparison with the AGB dataset generated in this study.

ID	Reference	Epoch	Spatial resolution	Map projection	Spatial extent
1	Saatchi et al., 2011 (Saatchi et al., 2011)	Early 2000s	1,000 m	Geographic	Pan-tropical between 40°N and 56°S
2	Baccini et al., 2012 (Baccini et al., 2012)	2007-2008	500 m	Sinusoidal	22°N, 22°S
3	GEOCARBON project (Santoro et al., 2015; Avitabile et al., 2016a)	2000-2010	1,000 m	Geographic	Global
4	Thurner et al., 2014 (Thurner et al., 2014)	2010	0.01°	Geographic	> 30°N
5	Liu et al., 2015 (Liu et al., 2015)	2010	0.25°	Geographic	Global
6	Kindermann et al., 2008 (Kindermann et al., 2008)	2000-2005	0.5°	Geographic	Global

Table S6. Legend of the CCI Land Cover dataset including the conversion rules to the forest and non-forest class and the definition of Plant Functional Types (PFT) used in this study.

Value	Label	Forest/non-forest label	PFT code
0	No data	No data	n/a
10	Cropland, rainfed	Non-forest	n/a
20	Cropland, irrigated or post-flooding	Non-forest	n/a
30	Mosaic cropland (>50%) / natural vegetation (tree, shrub, herbaceous cover (<50%)	Non-forest	n/a
40	Mosaic natural vegetation (tree, shrub, herbaceous cover) (>50%) / cropland (<50%)	Forest	5
50	Tree cover, broadleaved, evergreen, closed to open (>15%)	Forest	2
60	Tree cover, broadleaved, deciduous, closed to open (>15%)	Forest	4
70	Tree cover, needleleaved, evergreen, closed to open (>15%)	Forest	1
80	Tree cover, needleleaved, deciduous, closed to open (>15%)	Forest	3
90	Tree cover, mixed leaf type (broadleaved and needleleaved)	Forest	5
100	Mosaic tree and shrub (>50%) / herbaceous cover (<50%)	Forest	5
110	Mosaic herbaceous cover (>50%) / tree and shrub (<50%)	Non-forest	5
120	Shrubland	Non-forest	6
130	Grassland	Non-forest	n/a
140	Lichens and mosses	Non-forest	n/a
150	Sparse vegetation (tree, shrub, herbaceous cover) (<15%)	Non-forest	n/a
160	Tree cover, flooded, fresh or brackish water	Forest	n/a
170	Tree cover, flooded, saline water	Forest	n/a
180	Shrub or herbaceous cover, flooded	Non-forest	n/a
190	Urban areas	Non-forest	n/a
200	Bare areas	Non-forest	n/a
210	Water bodies	Non-forest	n/a
220	Permanent snow and ice	Non-forest	n/a

Table S7. Country/area statistics on forest area (in hectares), AGB (in Mg ha^{-1}), total AGB (in Mg) from this study and the FAO FRA of 2010. From the FAO FRA, the AGB was obtained as the ratio between total AGB and forest area for the year 2010. We estimated the total AGB from our dataset from the map of AGB, after masking for forest area using the CCI Land Cover dataset as reference. The column "FAO, AGB estimation" shows the procedure applied by each country to report AGB (1: AGB = GSV * IPCC default BCEF; 2: AGB = GSV * country specific BCEF(s); 3 = direct computation of AGB with allometric equations). BCEF stands for Biomass Conversion and Expansion Factor.

Country/area	Forest area [ha] This study	Forest area [ha] FAO FRA 2010	AGB [Mg ha-1] This study	AGB [Mg ha-1] FAO FRA 2010	Total AGB [Mg] This study	Total AGB [Mg] FAO FRA 2010	FAO AGB estimation method
Afghanistan	3654222	1350000	3	47	11512253	63450000	1
Albania	1240958	776300	62	94	76512037	72972200	2
Algeria	2131900	1492000	45	61	96718951	91012000	2
American Samoa	11149	17712	182	177	2028604	3135024	1
Andorra	27751	16000	125	0	3477852	0	0
Angola	76696056	58480000	77	128	5915953347	7485440000	1
Anguilla	0	5500	0	0	0	0	0
Antigua and Barbuda	20877	9800	82	0	1712441	0	0
Argentina	44028048	29400000	64	171	2816710661	5027400000	1
Armenia	1515082	331000	28	80	42271803	26480000	1
Aruba	48	420	0	0	12	0	0
Australia	106083374	149300000	85	63	9067829688	9405900000	0
Austria	4588587	3887000	145	160	664805497	621920000	3
Azerbaijan	2175753	936000	55	105	118783046	98280000	3
Bahamas	601374	515000	55	0	33304653	0	0
Bahrain	341	526	0	0	72	0	0
Bangladesh	1891724	1442000	93	99	176384634	142758000	1
Barbados	7633	8360	71	0	538936	0	0
Belarus	9117075	8630000	125	115	1143243825	992450000	1
Belgium	726379	677800	154	158	111953880	107092400	2
Belize	1914476	1393000	122	211	234278387	293923000	1
Benin	4418885	4561000	44	99	194246452	451539000	1
Bermuda	0	1000	0	0	0	0	0
Bhutan	3237084	3249000	116	161	375373497	523089000	2
Bolivia (Plurinational State of)	64659928	57196000	146	133	9413263444	7607068000	2
Bosnia and Herzegovina	3054069	2185000	128	115	389984454	251275000	2
Botswana	5408299	11351000	25	78	136276588	885378000	1
Brazil	470174912	519522000	195	212	91824690139	1.10139E+11	2
British Virgin Islands	7712	3640	107	0	821415	0	0

Brunei Darussalam	516882	380000	286	323	148079302	122740000	1
Bulgaria	4807786	3927000	107	86	515908131	337722000	2
Burkina Faso	2740022	5649000	27	86	74862045	485814000	1
Burundi	389034	172000	65	165	25408519	28380000	1
Cambodia	9144688	10094000	129	63	1179018223	635922000	1
Cameroon	37706120	19916000	173	232	6518400248	4620512000	2
Canada	468950048	310134000	73	88	34020393908	27291792000	3
Cape Verde	48653	85090	9	95	416998	8083550	1
Cayman Islands	3671	12700	0	0	65	0	0
Central African Republic	57350260	22605000	101	217	5771500765	4905285000	1
Chad	8808625	11525000	31	92	271978717	1060300000	1
Chile	25450816	16231000	142	138	3625193870	2239878000	2
China	225822736	206860000	60	48	13469023205	9929280000	2
Colombia	79387577	60499000	206	193	16329778410	11676307000	1
Comoros	144552	3000	78	203	11325976	609000	1
Congo	29066268	22411000	215	263	6261391507	5894093000	1
Cook Islands	2573	15500	0	0	0	0	0
Costa Rica	4548241	2605000	120	157	544286636	408985000	1
Côte d'Ivoire	13726208	10403000	73	350	1007956495	3641050000	3
Croatia	2639787	1920000	123	215	324391312	412800000	1
Cuba	5564204	2870000	62	135	345027078	387450000	1
Cyprus	240821	173182	54	27	12915566	4675914	2
Czech Republic	3000429	2657000	149	240	445762672	637680000	2
Democratic People's Republic of Korea	7670217	5666000	71	47	545000826	266302000	2
Democratic Republic of the Congo	191012544	154135000	176	219	33624377449	33755565000	1
Denmark	570651	544000	107	117	61015982	63648000	2
Djibouti	11605	5600	2	32	22630	179200	1
Dominica	71936	44660	159	0	11430369	0	0
Dominican Republic	2651071	1972000	83	99	220272659	195228000	2
Ecuador	18709058	9865000	194	0	3636116648	0	0
Egypt	4748	70000	8	168	35855	11760000	2
El Salvador	1526000	287000	61	0	92649991	0	0
Equatorial Guinea	2413634	1626000	265	214	638484745	347964000	1
Eritrea	1626972	1532000	2	0	2640273	0	0
Estonia	2821381	2217000	98	119	275397253	263823000	2
Ethiopia	31498944	12296000	58	30	1819713524	368880000	1

Falkland Islands (Malvinas)	0	0	0	0	0	0	0
Faroe Islands	18440	100	0	0	0	0	0
Fiji	1348486	1014080	70	0	94332337	0	0
Finland	24700788	22157000	71	64	1755639383	1418048000	2
France	15248251	15954000	136	124	2066574110	1978296000	2
French Guiana	8173948	8082000	274	350	2238012930	2828700000	3
French Polynesia	148559	155000	53	232	7894176	35960000	2
Gabon	24031272	22000000	259	211	6228345774	4642000000	1
Gambia	275530	480000	38	113	10594577	54240000	1
Georgia	4119326	2742290	124	123	508826089	337301670	2
Germany	11750143	11076000	162	195	1908828356	2159820000	2
Ghana	9355796	4940000	53	132	492863801	652080000	1
Gibraltar	0	0	0	0	0	0	0
Greece	4237905	3903000	83	34	353401229	132702000	1
Greenland	844134	220	0	0	0	0	0
Grenada	30726	16990	179	113	5509729	1919870	1
Guadeloupe	117625	63500	109	342	12830225	21717000	2
Guam	0	25880	0	109	0	2820920	1
Guatemala	8648557	3657000	96	124	830704365	453468000	3
Guernsey	0	200	0	0	0	0	0
Guinea	2605610	2022000	52	153	135486808	309366000	1
Guinea Bissau	18044326	6544000	59	85	1064102234	556240000	1
Guyana	19600644	15205000	258	189	5064594723	2873745000	3
Haiti	532128	101000	73	96	38889026	9696000	1
Holy See	0	0	0	0	0	0	0
Honduras	9854934	5192000	94	110	929631692	571120000	2
Hungary	1715300	2029000	127	112	217881554	227248000	2
Iceland	356102	29900	8	15	2736186	448500	2
India	75410520	68434000	70	48	5285606290	3284832000	2
Indonesia	140626992	94432000	226	221	31802611426	20869472000	1
Iran (Islamic Republic of)	6553564	11075000	22	39	147389720	431925000	1
Iraq	721212	825000	2	0	1143632	0	0
Ireland	869190	739000	84	49	73140972	36211000	3
Isle of Man	15680	3460	71	0	1119389	0	0
Israel	256430	154000	15	49	3824231	7546000	3
Italy	9950708	9149000	114	104	1136416655	951496000	2
Jamaica	846264	337100	101	233	85605026	78544300	3

Japan	26858030	24979000	133	0	3573630097	0	2
Jersey	0	600	0	0	0	0	0
Jordan	23544	97500	9	36	213259	3510000	1
Kazakhstan	20909026	3309000	17	64	365457784	211776000	2
Kenya	16346486	3467000	26	236	422750859	818212000	1
Kiribati	950	12150	0	0	0	0	0
Kuwait	178	6250	0	0	0	0	0
Kyrgyzstan	2770145	953800	26	87	71340258	82980600	2
Lao People's Democratic Republic	13888460	15751000	125	121	1740328201	1905871000	1
Latvia	3674419	3354000	98	123	361109884	412542000	2
Lebanon	129176	136900	20	21	2619548	2874900	1
Lesotho	663424	44000	19	90	12891854	3960000	1
Liberia	4681850	4329000	213	232	998753204	1004328000	1
Libyan Arab Jamahiriya	127569	217000	6	49	765928	10633000	1
Liechtenstein	9936	6900	144	119	1426856	821100	1
Lithuania	2220462	2160000	123	115	272337857	248400000	2
Luxembourg	93637	86750	160	201	14944634	17436750	2
Madagascar	54464428	12553000	66	222	3578884251	2786766000	1
Malawi	2695890	3237000	57	76	152527310	246012000	1
Malaysia	26279676	20456000	224	269	5889475117	5502664000	1
Maldives	819	900	0	0	0	0	0
Mali	5851609	12490000	29	37	167874339	462130000	1
Malta	742	347	2	288	1536	99936	1
Marshall Islands	62	12636	140	287	8722	3626532	3
Martinique	92606	48500	111	293	10250649	14210500	3
Mauritania	741962	242000	1	50	543228	12100000	1
Mauritius	77928	35000	43	113	3379867	3955000	1
Mayotte	35961	13815	138	0	4960252	0	0
Mexico	76207320	64802000	58	55	4457600865	3564110000	3
Micronesia (Federated States of)	8469	64129	0	500	0	32064500	3
Monaco	0	0	0	0	0	0	0
Mongolia	14076816	10898000	42	92	589480325	1002616000	1
Montenegro	911468	543000	95	91	86183961	49413000	3
Montserrat	7631	2500	111	0	848502	0	0
Morocco	3149671	5131000	13	71	40636208	364301000	3
Mozambique	46419612	39022000	47	69	2166354551	2692518000	1
Myanmar	37287604	31773000	130	92	4836832399	2923116000	1

Namibia	9557389	7290000	15	47	144444834	342630000	1
Nauru	0	0	0	0	0	0	0
Nepal	8601582	3636000	102	198	874618320	719928000	1
Netherlands	413740	365000	122	126	50554150	45990000	2
Netherlands Antilles	0	1180	0	0	0	0	0
New Caledonia	1411522	839000	49	126	69826430	105714000	3
New Zealand	9859323	8269000	148	251	1455114743	2075519000	3
Nicaragua	10481614	3114000	95	192	999787494	597888000	1
Niger	2315668	1204000	0	50	986447	60200000	1
Nigeria	25437620	9041000	70	206	1768486428	1862446000	1
Niue	19816	18600	0	0	0	0	0
Norfolk Island	0	460	0	0	0	0	0
Northern Mariana Islands	0	30319	0	158	0	4790402	3
Norway	18397766	10065000	60	67	1096308894	674355000	3
Occupied Palestinian Territory	89118	9170	2	0	184904	0	0
Oman	38095	2000	0	0	8879	0	0
Pakistan	6763130	1687000	17	198	115017365	334026000	1
Palau	0	40303	0	416	0	16766048	3
Panama	6170112	3251000	137	194	846653513	630694000	1
Papua New Guinea	41573856	28726000	249	142	10369854160	4079092000	1
Paraguay	21212386	17582000	67	0	1411768926	0	0
Peru	84221336	67992000	228	216	19206599876	14686272000	1
Philippines	14421642	7665000	138	149	1996715273	1142085000	1
Pitcairn	0	3500	0	0	0	0	0
Poland	10065562	9337000	145	158	1460388233	1475246000	2
Portugal	5199677	3456000	31	45	163050379	155520000	3
Puerto Rico	614071	552000	108	89	66201029	49128000	3
Qatar	2751	0	0	0	509	0	0
Republic of Korea	4873702	6222000	93	68	452574602	423096000	2
Republic of Moldova	266891	386000	122	129	32585374	49794000	1
Réunion	166294	88000	27	120	4484080	10560000	3
Romania	7760522	6573000	119	163	922592525	1071399000	2
Russian Federation	1014226416	809090000	63	64	64098825508	51781760000	2
Rwanda	393168	435000	101	156	39716213	67860000	2
Saint Barthélemy	0	0	0	0	0	0	0
Saint Helena, Ascension and Tristan da Cunha	3590	2000	0	0	0	0	0

Saint Kitts and Nevis	17879	11000	89	0	1586142	0	0
Saint Lucia	56638	47000	145	0	8210233	0	0
Saint Martin (French part)	0	1000	0	0	0	0	0
Saint Pierre and Miquelon	0	2900	0	0	0	0	0
Saint Vincent and the Grenadines	34446	26700	146	0	5045955	0	0
Samoa	173001	171000	117	0	20169446	0	0
San Marino	0	0	0	0	0	0	0
Sao Tome and Principe	89255	27000	11	240	942638	6480000	2
Saudi Arabia	73913	977000	1	10	88820	9770000	1
Senegal	5641965	8473000	26	65	147131827	550745000	2
Serbia	3371569	2713000	96	147	324478202	398811000	2
Seychelles	4993	40700	0	150	0	6105000	1
Sierra Leone	3220940	2726000	85	136	273108904	370736000	1
Singapore	0	2300	0	0	0	0	0
Slovakia	2425363	1933000	142	177	344050389	342141000	3
Slovenia	1332997	1253000	156	222	208276171	278166000	2
Solomon Islands	2715396	2213000	163	141	443877407	312033000	1
Somalia	6955301	6747000	10	100	66492552	674700000	1
South Africa	14097394	9241000	41	147	572172340	1358427000	2
Spain	19809412	18173000	53	37	1043202462	672401000	3
Sri Lanka	2528773	1860000	98	58	246758076	107880000	1
Sudan	38980024	69949000	12	33	480994396	2308317000	1
Suriname	14120867	14758000	277	368	3916147106	5430944000	3
Svalbard and Jan Mayen Islands	5207	0	0	0	0	0	0
Swaziland	671816	563000	60	67	40595734	37721000	1
Sweden	32367846	28203000	80	72	2596764176	2030616000	3
Switzerland	1577975	1240000	151	189	238722509	234360000	2
Syrian Arab Republic	650013	491000	16	0	10310759	0	0
Tajikistan	742176	410000	2	10	1781323	4100000	2
Thailand	16957310	18972000	123	78	2081803164	1479816000	1
The former Yugoslav Republic of Macedonia	1245727	998000	76	102	94122588	101796000	1
Timor Leste	609200	742000	95	0	58120665	0	0
Togo	2456132	287000	54	0	132214765	0	0
Tokelau	0	0	0	0	0	0	0
Tonga	29767	9000	148	202	4401121	1818000	1
Trinidad and Tobago	411457	226400	201	147	82520214	33280800	1

Tunisia	390022	1006000	57	14	22358603	14084000	2
Turkey	27021788	11334000	48	115	1294076400	1303410000	2
Turkmenistan	202381	4127000	0	4	45616	16508000	1
Turks and Caicos Islands	45245	34400	19	0	876833	0	0
Tuvalu	0	1000	0	0	0	0	0
Uganda	5960322	2988000	58	61	346516015	182268000	3
Ukraine	9465297	9705000	126	126	1192035841	1222830000	2
United Arab Emirates	31632	317300	0	74	6018	23480200	2
United Kingdom	4967168	2881000	65	81	324990924	233361000	2
United Republic of Tanzania	39423588	33428000	55	104	2171233215	3476512000	1
United States of America	330577345	304022000	96	106	31886895696	32226332000	2
United States Virgin Islands	16872	20230	102	43	1728412	869890	2
Uruguay	2681469	1744000	57	0	154008122	0	0
Uzbekistan	519118	3275500	6	9	2904266	29479500	1
Vanuatu	1141952	440000	127	0	144804424	0	0
Venezuela (Bolivarian Republic of)	56874372	46275000	195	0	11088608623	0	0

Table S8. Region-specific reasons for AGB retrieval errors.

Region	Result	Explanation
Alaska	Underestimation	The maximum biomass used to constrain the retrieval in this study was derived from (Blackard et al., 2008). This value was found to be lower than maximum AGB from the inventory database.
Nova Scotia, Canada	Reduced variability	The simplified modelling of SAR backscatter as a function of GSV caused overestimation in the low biomass range (around 50 Mg ha^{-1}) and underestimation in the high biomass range (around 100 Mg ha^{-1})
Yucatan, Mexico	Reduced variability	The simplified modelling of SAR backscatter as a function of GSV caused overestimation in the low biomass range (around 50 Mg ha^{-1}) and underestimation in the high biomass range (around 150 Mg ha^{-1})
Wet tropics, Amazon and Central Africa	Underestimation	The AGB was estimated from a single L-band SAR backscatter mosaic. Because of the very weak sensitivity to AGB of L-band backscatter for AGB above 150 Mg ha^{-1} (< 0.2 dB), (i) uncorrected topographic distortions in backscatter, (ii) image post-processing to reduce systematic artefacts affecting the L-band backscatter mosaic and (iii) uncertainty in the model parameter estimates lead to underestimation of AGB above 250 Mg ha^{-1}.
Northeast Spain	Overestimation	Unrealistic high values because of very high maximum biomass associated with the neighbouring regions of the Pyrenees.
Sweden	Reduced variability	The simplified modelling of SAR backscatter as a function of GSV caused overestimation in the low biomass range (around 50 Mg ha^{-1}) and underestimation in the high biomass range (around 150 Mg ha^{-1})
Croatia	Underestimation	Strong forest fragmentation and maximum biomass lower than values reported by the plot inventory dataset.
Kenya and Ethiopia	Underestimation	Maximum biomass higher than the value assigned, causing underestimation for AGB > 150 Mg ha-1 in mountain forest ecosystems.
Kenya and Ethiopia	Underestimation	Maximum biomass higher than the value assigned causing underestimation for AGB > 150 Mg ha-1 in mountain forest ecosystems.
Madagascar	Underestimation	The AGB was estimated from a single L-band SAR backscatter mosaic. Because of the very weak sensitivity of L-band backscatter for AGB above 150 Mg ha^{-1} (< 0.2 dB), (i) uncorrected topographic distortions in backscatter, (ii) image post-processing to reduce systematic artefacts affecting the L-band backscatter mosaic and (iii) uncertainty in the model parameters estimates lead to underestimation of biomass above 250 Mg ha^{-1}.
Vietnam	Reduced variability	The simplified modelling of SAR backscatter as a function of GSV caused overestimation in the low biomass range (around 50 Mg ha^{-1}) and underestimation in the high biomass range (around 250 Mg ha^{-1})
Western Australia	Underestimation	The simplified modelling of SAR backscatter as a function of GSV caused underestimation throughout the range of AGBs
Eastern Australia	Reduced variability	The simplified modelling of SAR backscatter as a function of GSV caused overestimation in the low biomass range (around 100 Mg ha^{-1}) and underestimation in the high biomass range (above 250 Mg ha^{-1}).

Table S9. Legend of wood density estimation methods.

Description	Id
Landscape-based model, with gap-filled TRY database	1
Landscape-based model, with alternative gap-filling of the TRY database	2
Landscape-based model, with original TRY database	3
Plot/tree-level estimation, with original TRY database	4
Plot/tree-level estimation, with gap-filled TRY database	5
Plot/tree-level estimation, with gap-filled TRY database and leaf-type information	6
Plot/tree-level estimation, with original TRY database and leaf-type information	7

Table S10. Legend of the Köppen-Geiger classification (Kottek et al., 2006)

ID	Code	Description
1	Af	Equatorial rainforest, fully humid
2	Am	Equatorial monsoon
3	As	Equatorial savannah with dry summer
4	Aw	Equatorial savannah with dry winter
5	BSh	Steppe climate, hot arid
6	HSk	Steppe climate, cold arid
7	BWh	Desert climate, hot arid
8	BWk	Desert climate, cold arid
9	Cfa	Warm temperate climate, fully humid, hot summer
10	Cfb	Warm temperate climate, fully humid, warm summer
11	Cfc	Warm temperate climate, fully humid, cool summer
12	Csa	Warm temperate climate with dry summer, hot summer
13	Csb	Warm temperate climate with dry summer, warm summer
14	Csc	Warm temperate climate with dry summer, cool summer
15	Cwa	Warm temperate climate with dry winter, hot summer
16	Cwb	Warm temperate climate with dry winter, warm summer
17	Cwc	Warm temperate climate with dry winter, cool summer
18	Dfa	Snow climate, fully humid, hot summer
19	Dfb	Snow climate, fully humid, cool summer
20	Dfc	Snow climate, fully humid, warm summer; 20
21	Dfd	Snow climate, fully humid, extremely continental
22	Dsa	Snow climate with dry summer, hot summer
23	Dsb	Snow climate with dry summer, warm summer
24	Dsc	Snow climate with dry summer, cool summer
25	Dwa	Snow climate with dry winter, hot summer
26	Dwb	Snow climate with dry winter, warm summer
27	Dwc	Snow climate with dry winter, cool summer
28	Dwd	Snow climate with dry winter, extremely continental
29	EF	Frost climate
30	ET	Tundra climate

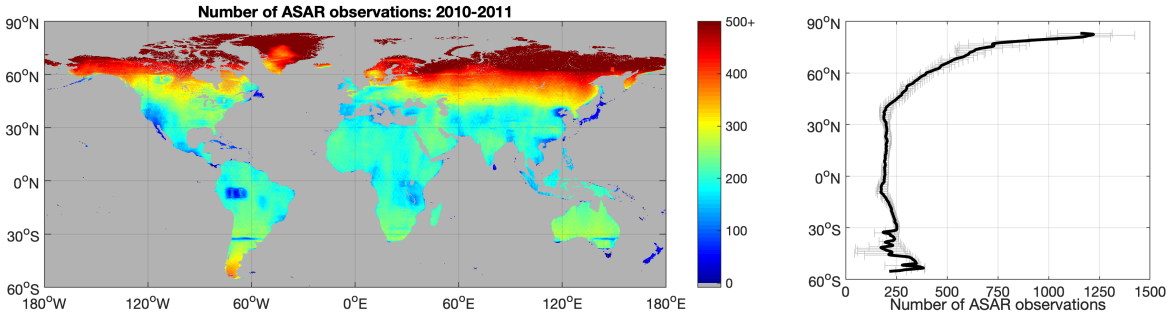

Figure S1. Number of Envisat ASAR observations acquired over land in 2010 and 2011 (left panel) and latitudinal profile of the average number of observations (right panel). The colour bar of the map was truncated at 500 observations to enhance the colour contrast. The complete representation of the number of observations available is illustrated in the panel on the right-hand side. The horizontal bars in the panel of the latitudinal profile represent the interquartile range of the number of observations at each given latitude.

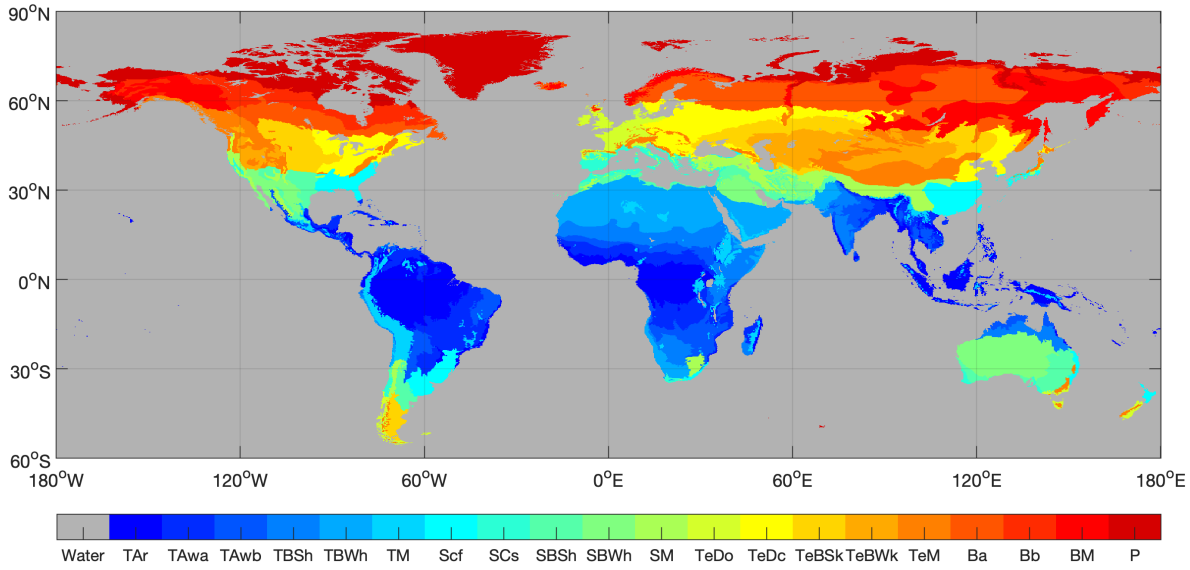

Figure S2. FAO Global Ecological Zones map. Legend: TAr = Tropical rainforest; TAwa = Tropical moist deciduous forest; TAwb = Tropical dry forest; TBSh = Tropical shrubland; TBWh = Tropical desert; TM = Tropical mountain; SCf = Subtropical humid; SCs = Subtropical dry; SBSh = Subtropical steppe; SBWh = Subtropical desert; SM = Subtropical mountain; TeDo = Temperate oceanic; TeDc = Temperate continental; TeBSk = Temperate steppe; TeBWk = Temperate desert; TeM = Temperate mountain; Ba = Boreal coniferous; Bb = Boreal tundra woodland; BM= Boreal mountain; P = Polar.

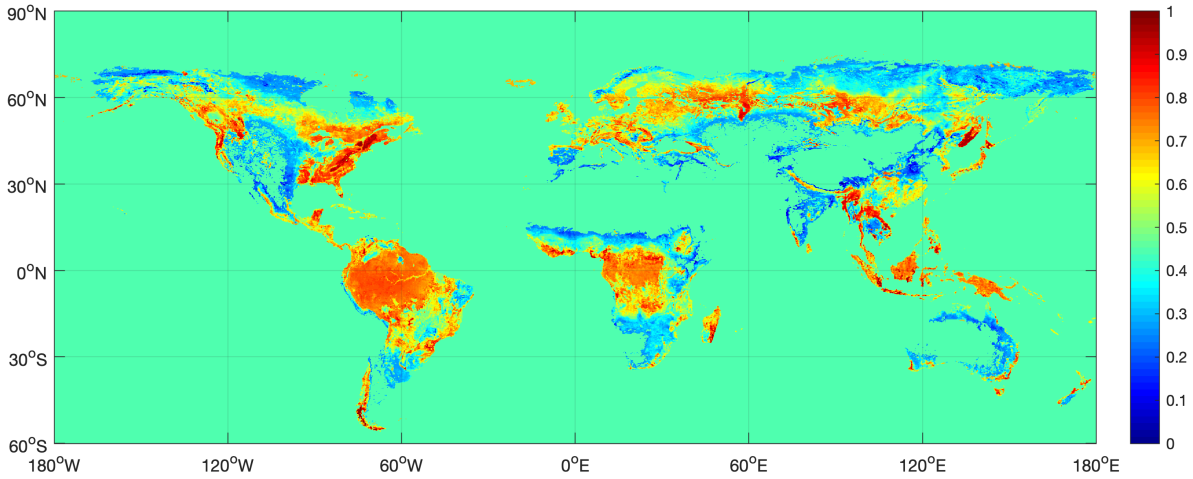

Figure S3. Raster dataset of the weights applied to the BIOMASAR-L GSV estimates, w_L. The weights applied to the BIOMASAR-C+ estimates are given by 1 - w_L.

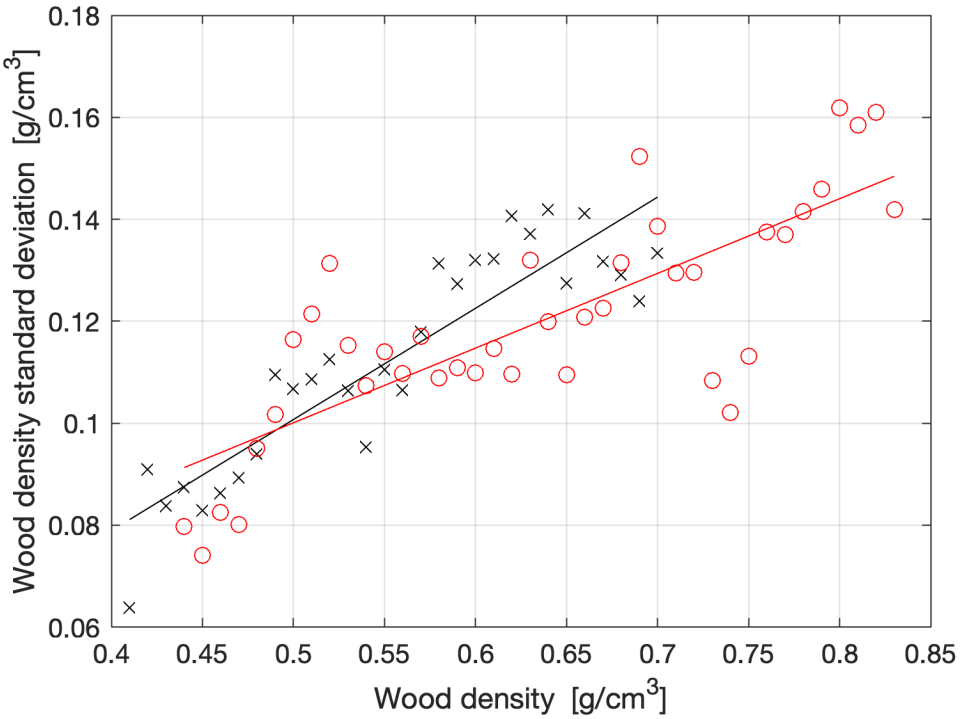

Figure S4. Relating wood density (predicted) to an estimate of standard deviation derived from the corresponding values of observed wood density. Dark markers and line refer to the plot-level approach for estimating wood density (model number 5 in Table S9). Red markers and line refer to the landscape-based approach for estimating wood density (model number 2 in Table S9). The linear model represented by the black line: δWD = 0.2181*WD-0.0083. The linear model represented by the red line: δWD = 0.1465*WD+0.0268.

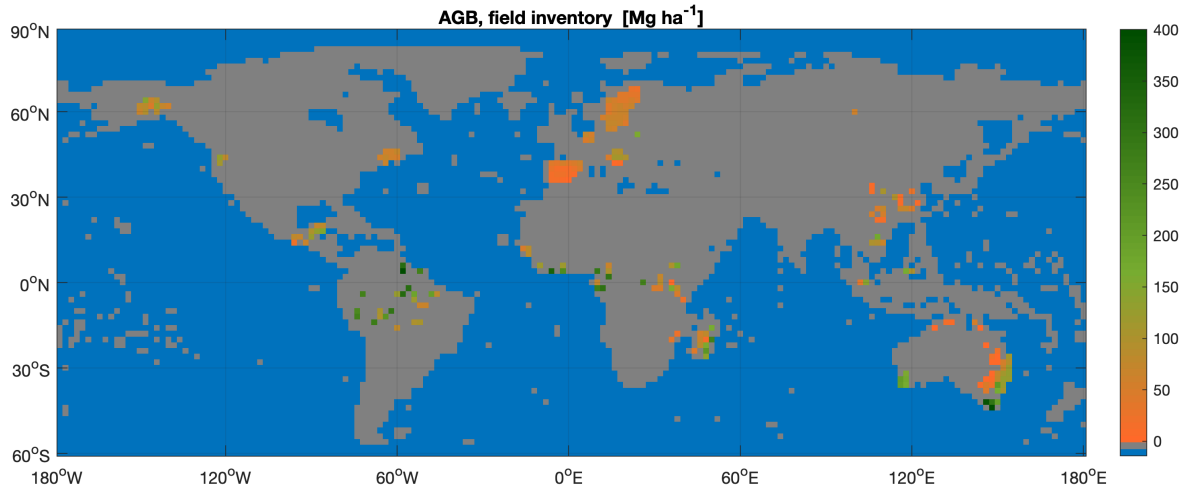

Figure S5. The spatial distribution of AGB measurements forming the database of observations used to validate the AGB estimates from this study. The colour bar has been truncated at 400 Mg ha^{-1} to increase contrast.

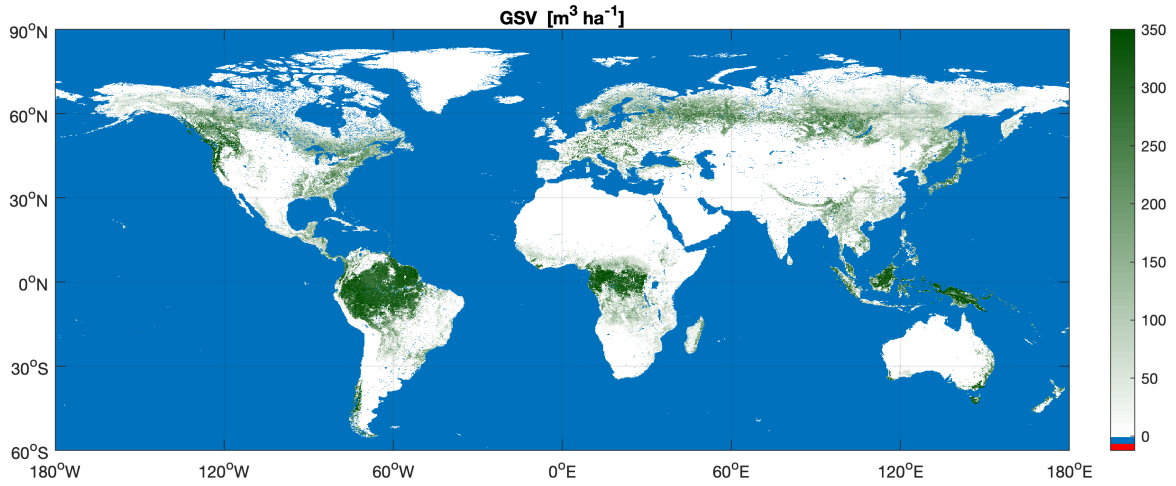

Figure S6. Spatially explicit estimates of GSV from this study. The colour bar has been truncated at 350 m^3 ha^{-1} to increase contrast.

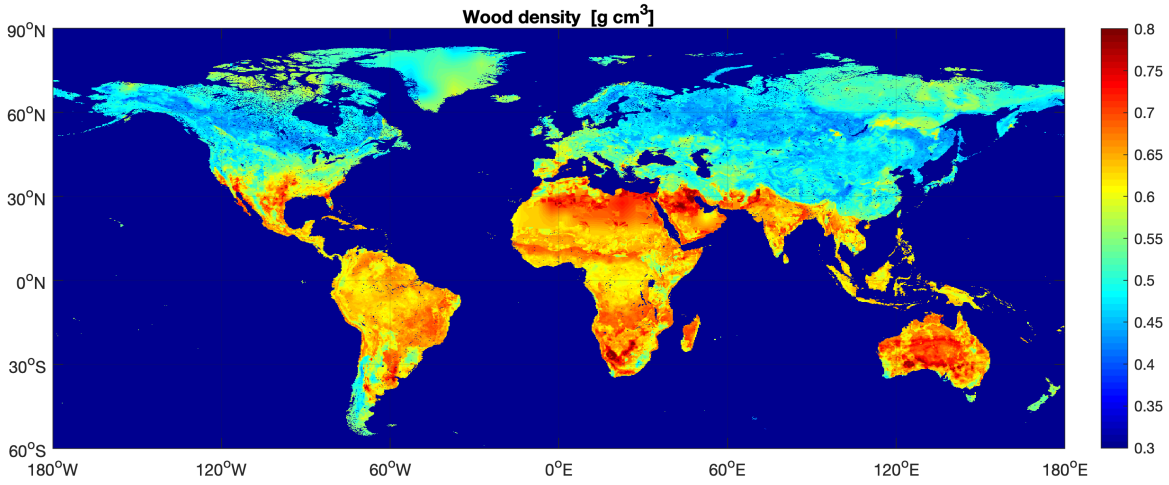

Figure S7. Spatially explicit estimates of wood density from this study.

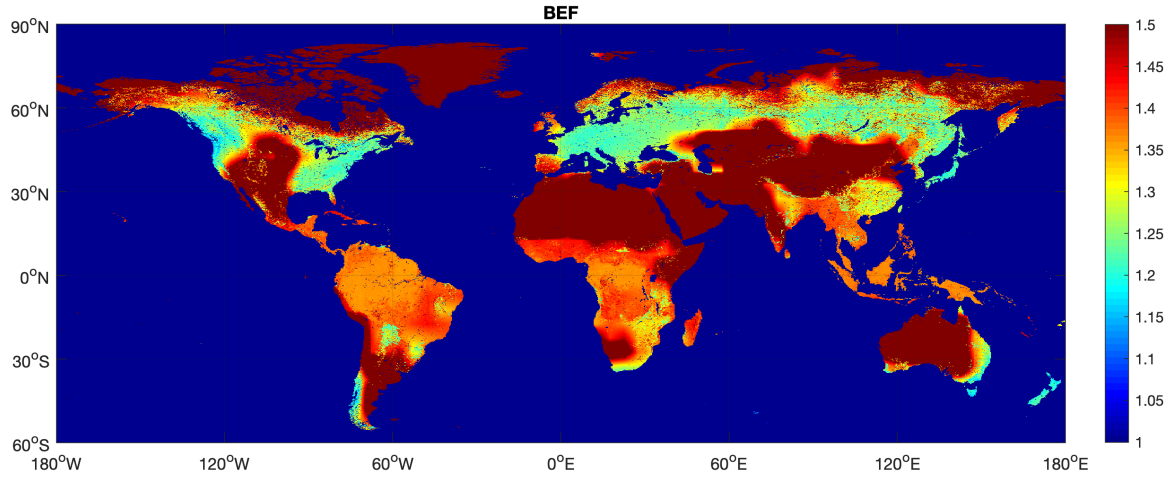

Figure S8. Map of the Biomass Expansion Factors from this study.

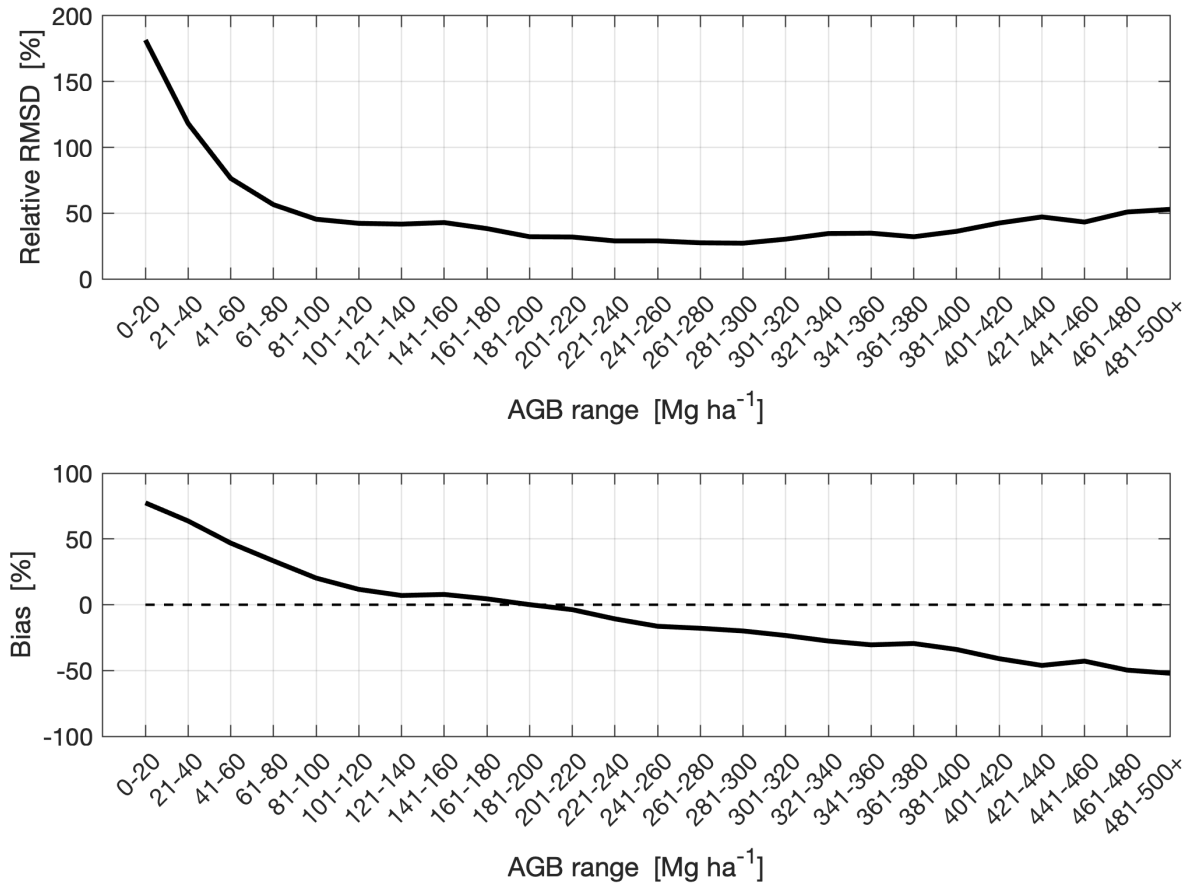

Figure S9. Detailing the RMSD and bias for the 0.1°-large grid cells per AGB level.

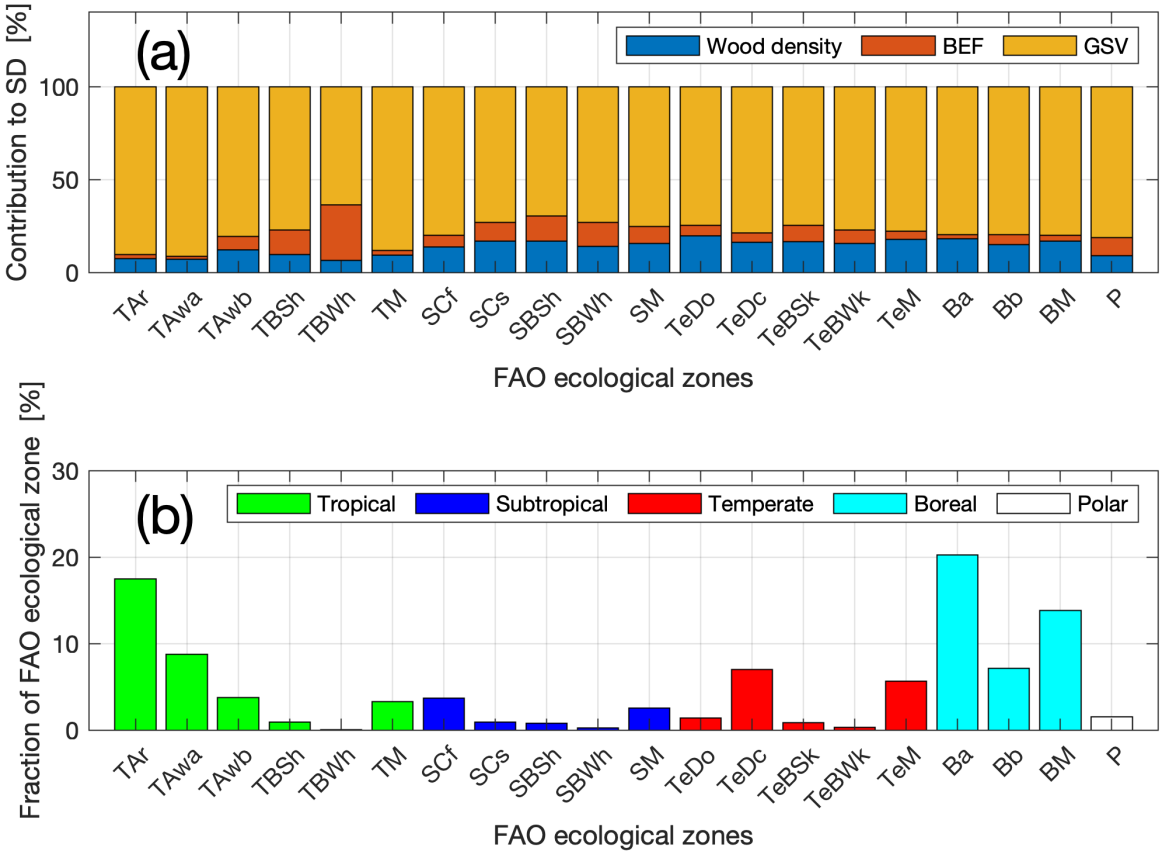

Figure S10. Panel (a) shows the contribution to the AGB percentage standard deviation (SD from (i) the retrieval model and remote sensing observations (GSV), (ii) the estimates of wood density and (iii) the estimates of the BEF, for each FAO Global Ecological Zone. The fraction of each ecozone to the global land surface is shown in panel (b). For the legend of the FAO ecological zones, refer to Table S2.

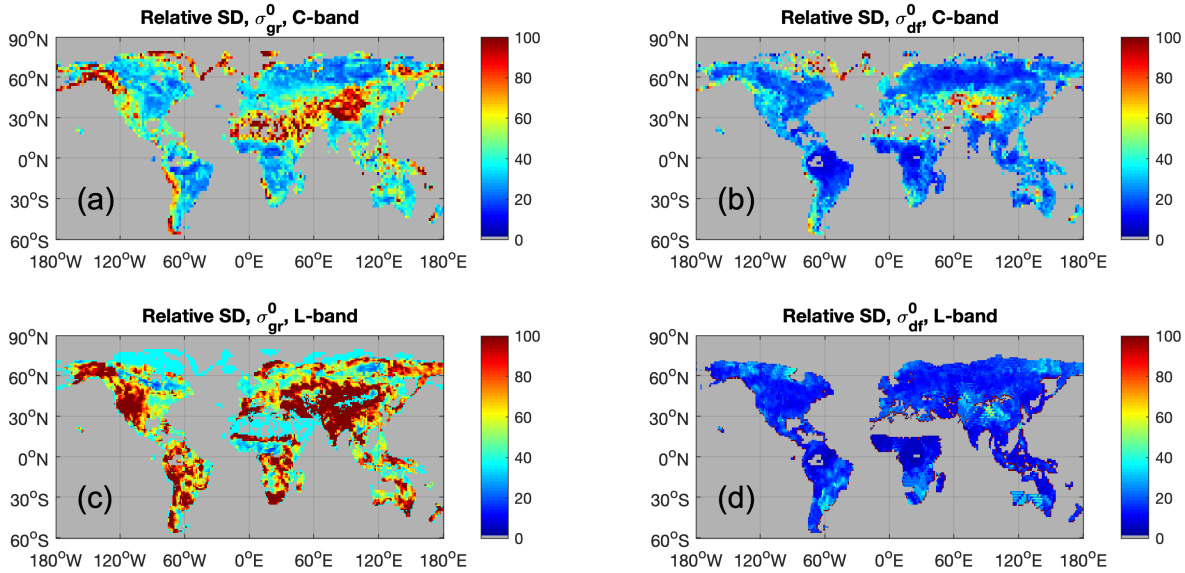

Figure S11. Standard deviation of the model parameter σ^0_{gr} relative to its estimate ($\delta\sigma^0_{gr}$ / σ^0_{gr}) expressed in % units for the C-band Envisat ASAR (a) and the L-band ALOS PALSAR (c) datasets. Standard deviation of the model parameter σ^0_{df} relative to its estimate ($\delta\sigma^0_{df}$ / σ^0_{df}) expressed in % units for the C-band Envisat ASAR (b) and the L-band ALOS PALSAR (d) dataset. Note that the uncertainty of the model parameter σ^0_{df} can be considered a proxy for the σ^0_{veg} parameter, Eq. (S2). For the C-band examples, we used the median values of $\delta\sigma^0_{gr}$, σ^0_{gr}, $\delta\sigma^0_{df}$ and σ^0_{df}.

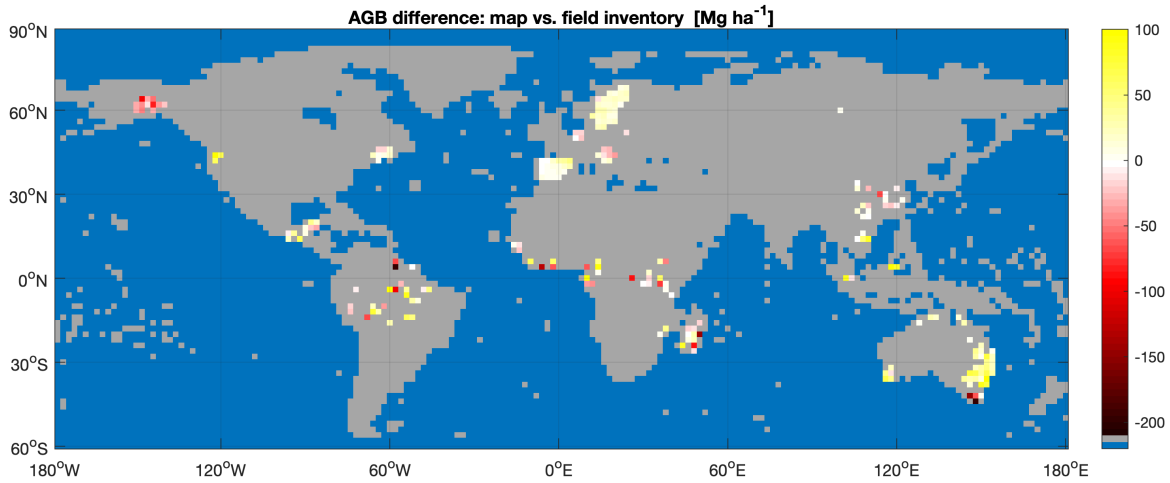

Figure S12. Difference between AGB estimated in this study and values from forest inventory measurements at the level of 0.1° averages. The colour bar has been truncated at between -200 Mg ha^{-1} and 100 Mg ha^{-1} to highlight spatial patterns.

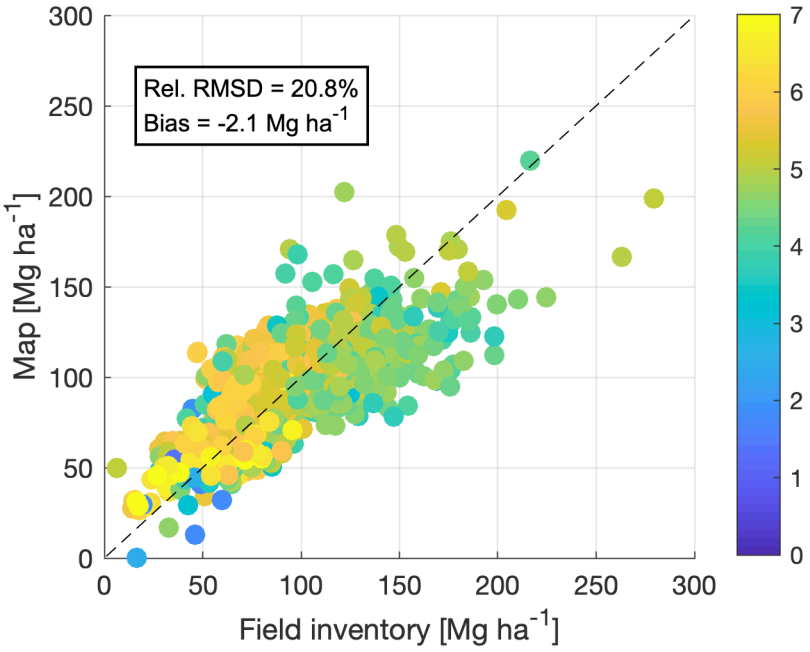

Figure S13. Scatter plot of map average vs. field inventory AGB for each Forest Management Unit (FMU) of the State Forest Register (SFR) of Russia. The circles are coloured in terms of the FMU's forest area, represented in the colour bar on a logarithmic scale. FMUs were largest in Siberia and the Far East region were AGB was low (yellowish circles). In contrast, the smallest units and the highest biomass stocks are in European Russia (greenish circles).

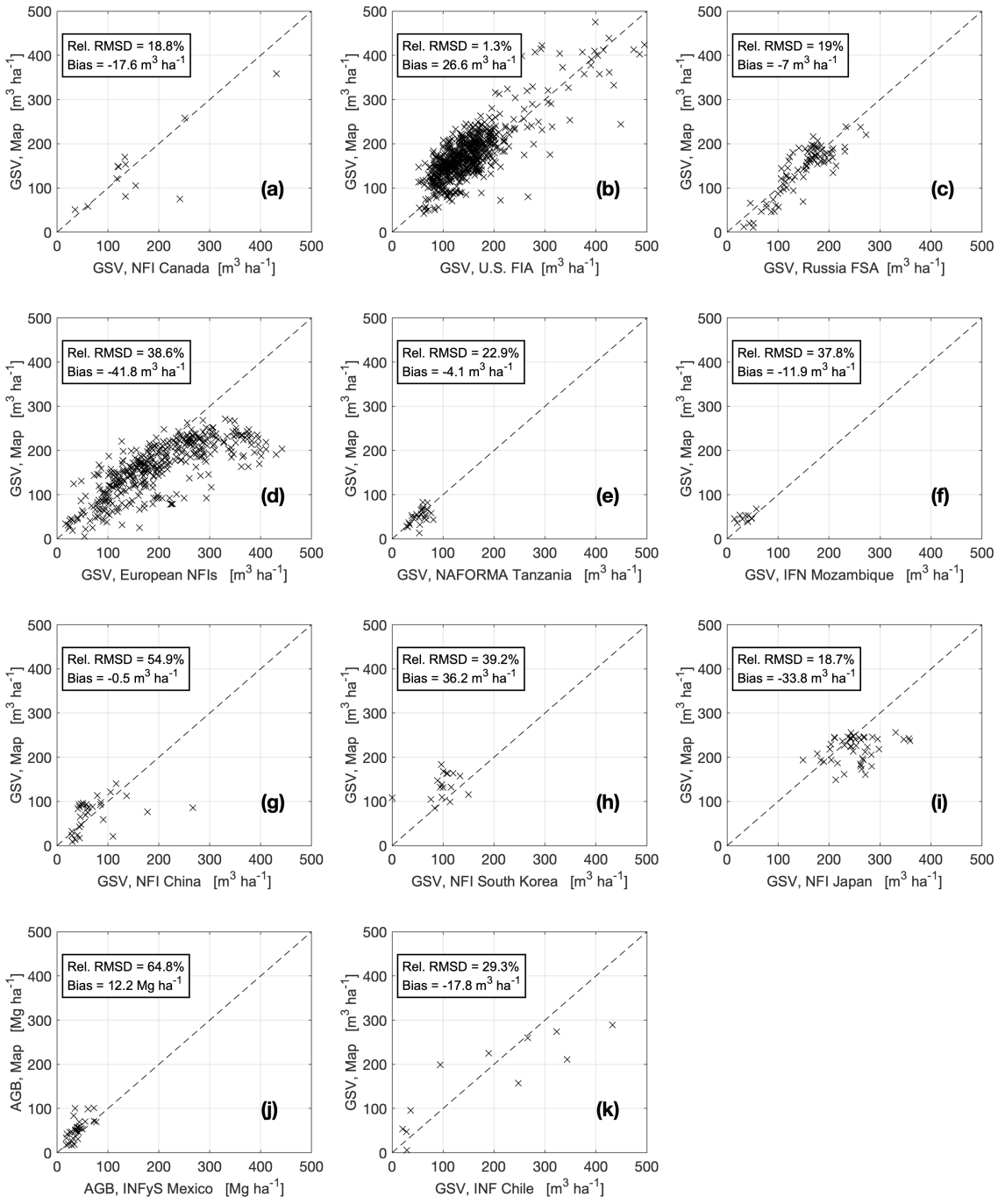

Figure S14. Comparison of GSV or AGB averages from this study with averages computed from national forest inventory data or published by national forest inventories. Panel (a): Canadian NFI, 11 ecoregions (Gillis et al., 2005). Panel (b), United States Forest Inventory Analysis Database (FIADB), 652 counties having at least 50% of forest cover and less than 10% standard error (Forest Inventory EVALIDator web-application version 1.6.0.00). Panel (c): Russian State Forest Register (FSA), 82 administrative regions (Santoro et al., 2015). Panel (d) European NFIs, 388 provinces in 27 countries (Santoro et al., 2015). Panel (e): National Forest Monitoring and Assessment (NAFORMA) of Tanzania, 25 states (Ministry of Natural Resources and Tourism, 2015). Panel (f): Inventário Florestal Nacional (IFN) of the Republic of Mozambique, 10 provinces (Marzoli, 2007). Panel (g): China's 7th NFI, 31 provinces (Zhu, 2010). Panel (h): Republic of Korea NFI, 17 units (KFS, 2010). Panel (i): Japan's NFI, 46 provinces (Kitahara et al., 2009). Panel (j): Mexico's NFI (INFyS), 32 states (Santoro et al., 2015). Panel (k): Chile's Instituto Forestal (INFOR), 11 regions (INFOR, 2015).

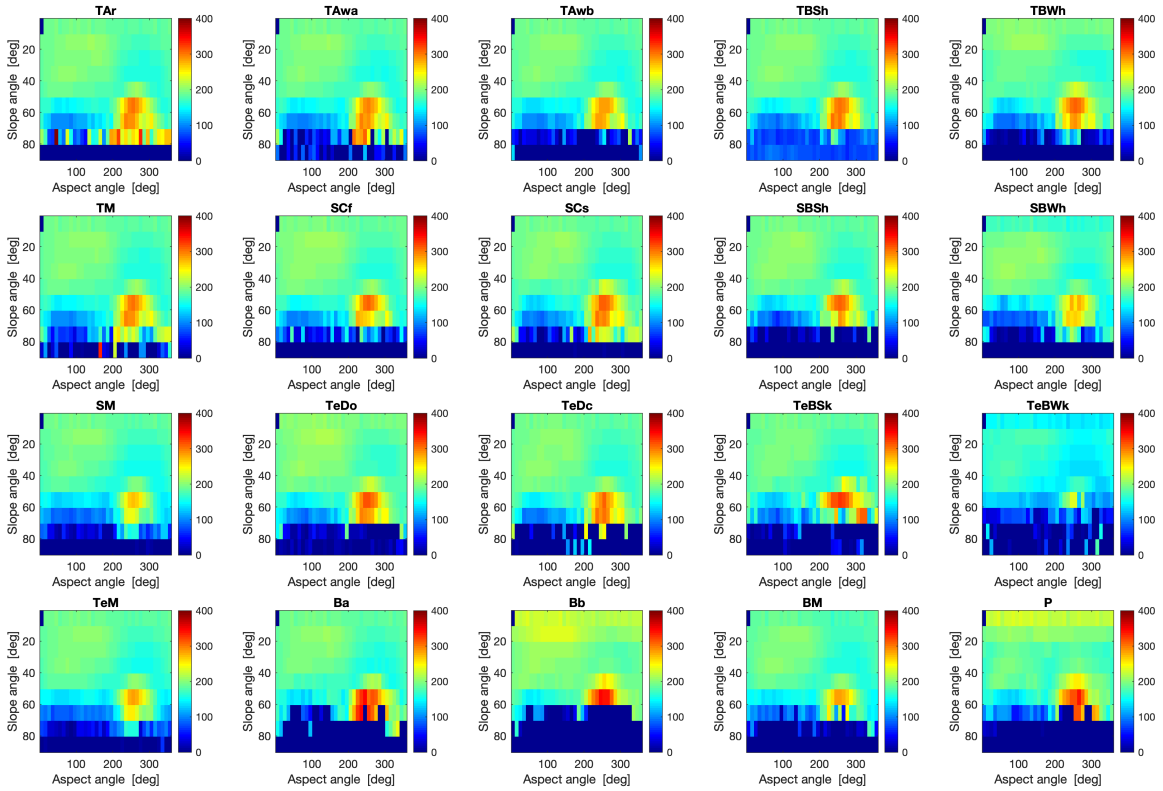

Figure S15. Average AGB after binning our estimates by terrain slope angle and aspect angle in 10° wide intervals and after stratification by FAO Global Ecological Zones. Refer to Table S5 for the legend of the FAO Global Ecological Zones. Terrain slope angle is defined as the angle between the vector normal to the pixel surface and the nadir direction. Terrain aspect angle is defined as the angle between the vector normal to the pixel surface projected on the ground and the North direction. For reference, terrain slopes facing the look direction of ALOS PALSAR have an aspect angle of approximately 260°. Terrain slopes looking away from the direction of sight of ALOS PALSAR have an aspect angle of approximately 80°. The effect of uncompensated topography on the ALOS PALSAR backscatter is visible in the form of strong AGB differences for slopes steeper than 30° when the average AGB for slopes facing the radar is consistently higher than the corresponding values estimated for slopes facing away from the radar.

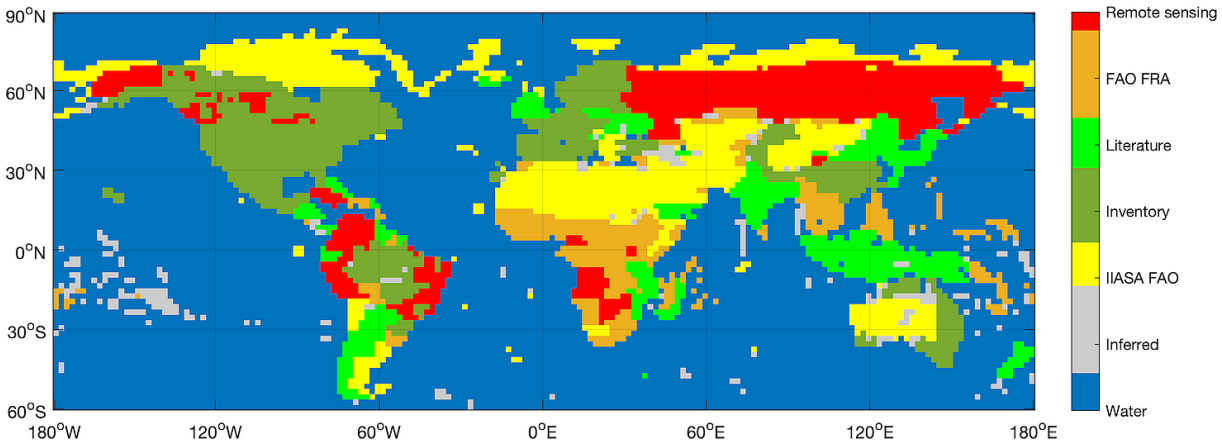

Figure S16. Map detailing the origin of the values used to generate an estimate of the biomass of dense forests at the spatial scale of 2°.

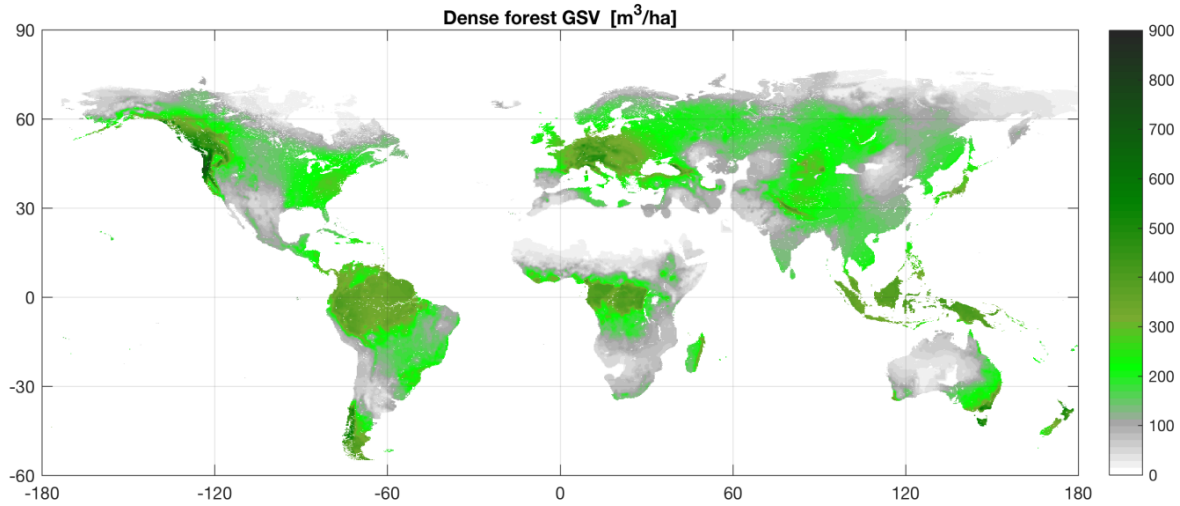

Figure S17. Map of the GSV of dense forests with a spatial resolution of 0.2°.

Figure S18. Distribution of wood density datasets from different sources. Values in parenthesis give the number of records of wood density in each database. Overall, these databases report wood density for a total of 4,952 species, showing a median number of two records per species.

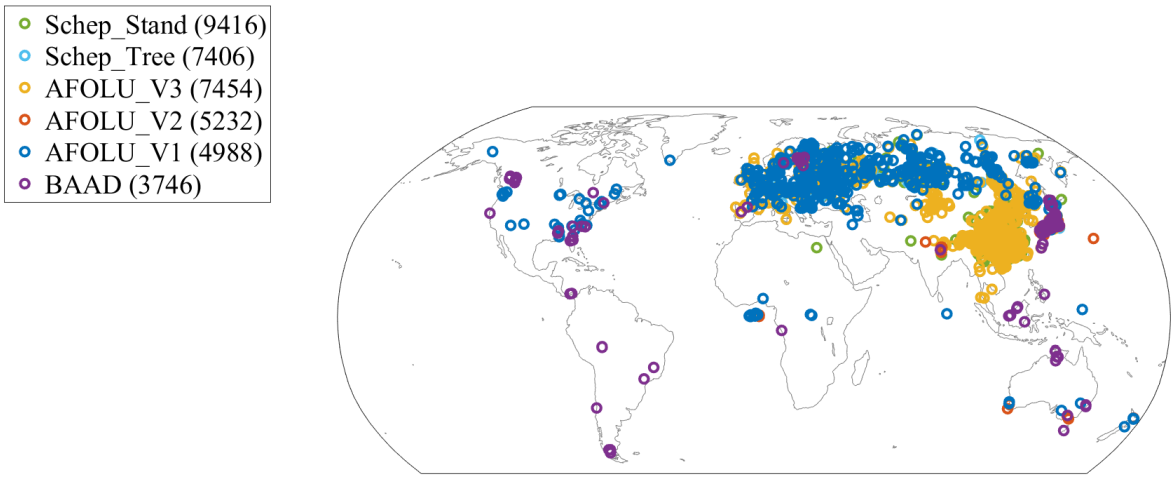

Figure S19. Distribution of allometric measurements from the different sources used to estimate AGB as a function of stem mass and other covariates. Values in parenthesis give the number of records in each database.

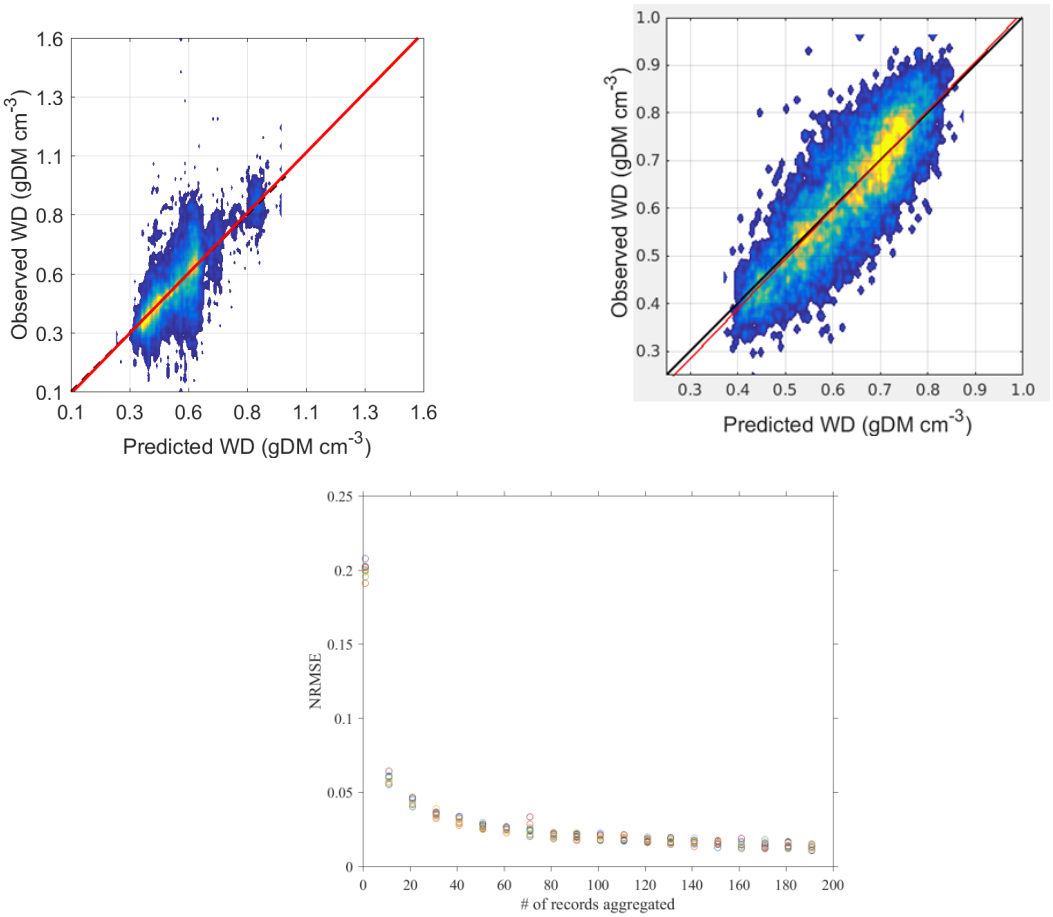

Figure S20. Top: density scatterplots of predictions of WD for the best tree/plot statistical model found (not gap-filled data and using leaf type/phenology as a covariate, top left) and for the landscape level estimates (top right). The regression line (red) almost overlaps the 1:1 line (dashed black line). Bottom: changes in root mean squared error, normalized by the mean in the observations with increasing number of aggregated records. This behaviour is observed in all the statistical models that were investigated. All the above tree/plot results are on cross-validated predictions.

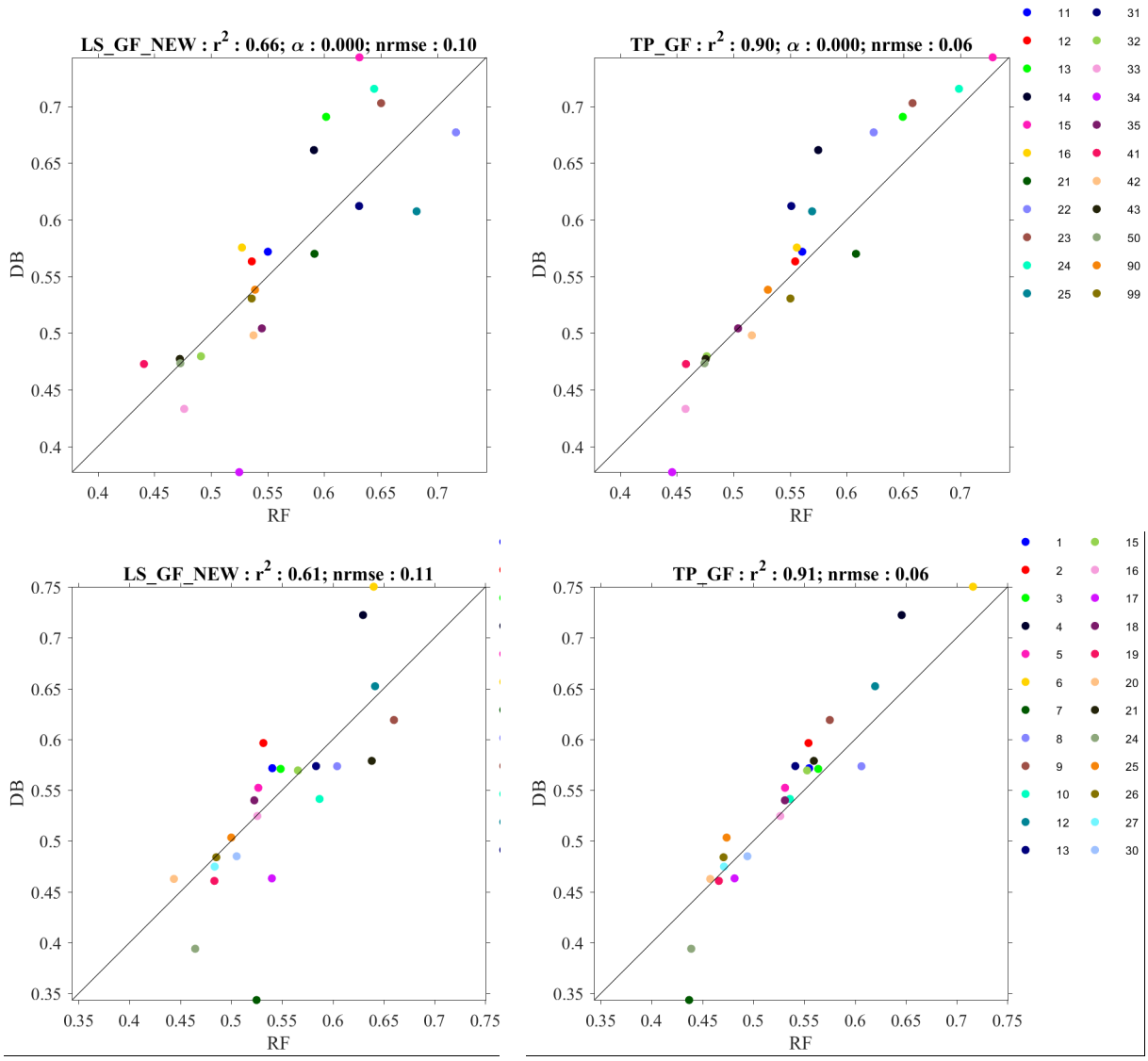

Figure S21. Comparison between predicted (RF) and observed (DB) wood density per FAO Global Ecological Zone (top, see Table S2 for the legend) and bioclimatic class (bottom, see Table S10 for the legend) for LS_GF (landscape scale using gap-filled data, left) and TP_GF (tree/plot based estimates using gap-filled data, right). These results show that, despite a locally poorer explained variance in the wood density predictions, the overall global biogeographic gradients are well explained and no substantial biases are observed per class/region.

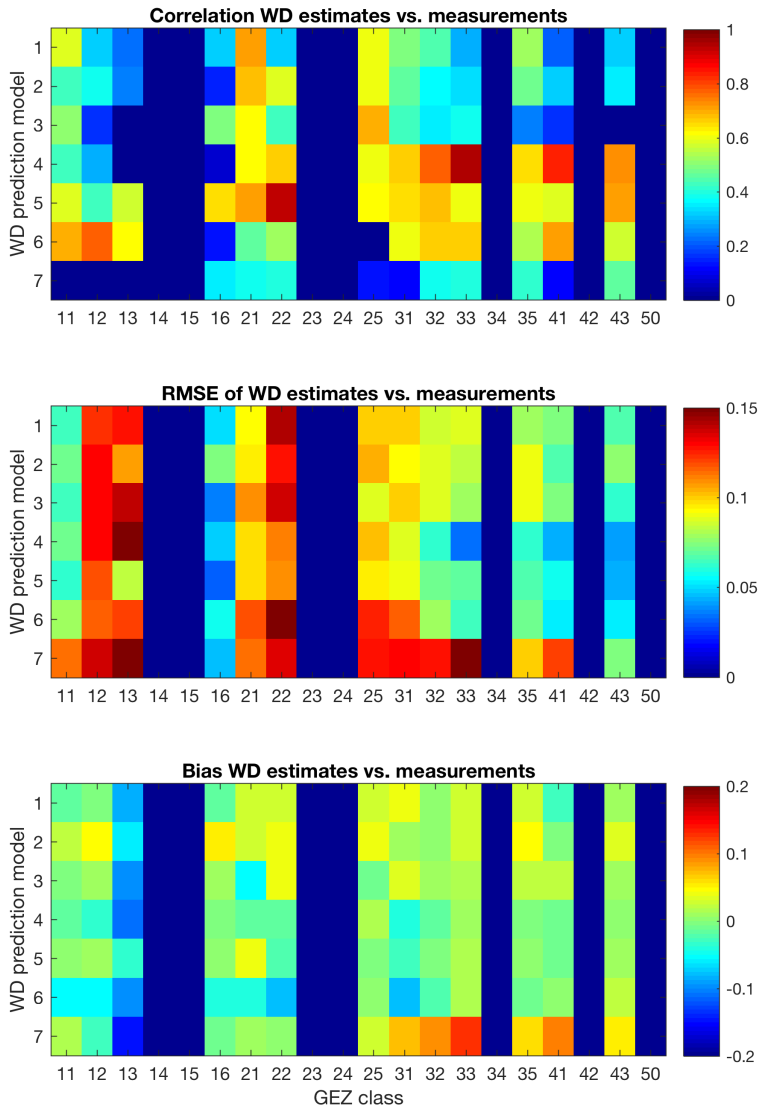

Figure S22. Values of the Pearson's correlation coefficient (top), RMSE (centre) and bias (bottom) between predicted and observed wood density for a given FAO Global Ecological zone (for the legend, see Table S2) and estimation method (for the legend, see Table S9).

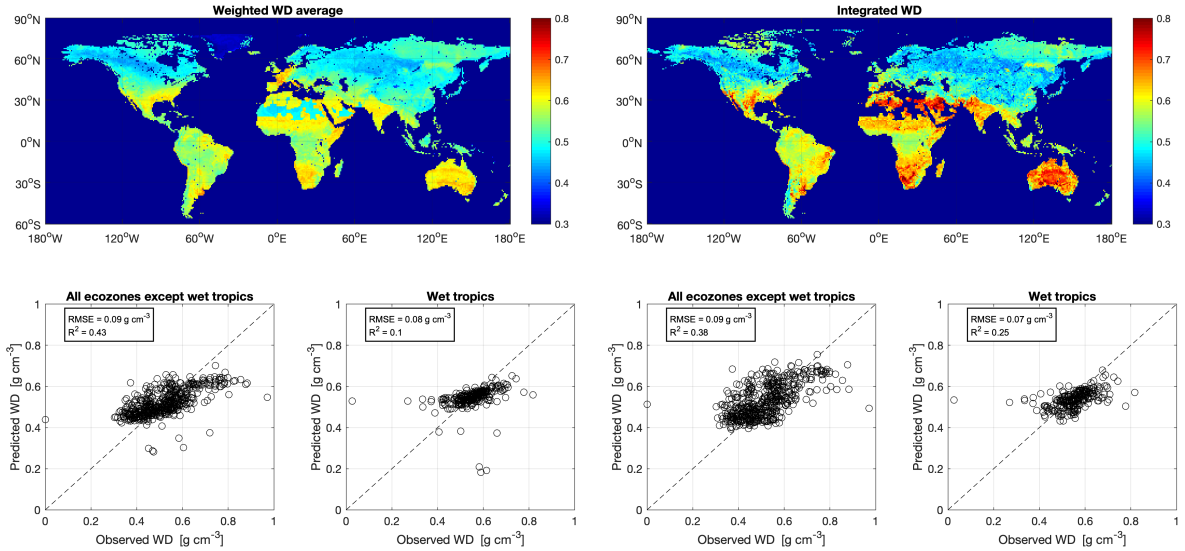

Figure S23. Spatially explicit estimates of wood density (WD) obtained from weighted average of predictions (top row, panel on the left hand-side) and integration of multiple predictions (top row, panel on the right hand-side). Observed and predicted wood densities for the weighted average (bottom row, panels on the left hand-side) and for the integrated dataset (bottom row, panel on the right hand-side) Only wood density samples characterized by at least 10 observations were retained to generate the scatterplots.

References

Askne, J., Dammert, P. B. G., Ulander, L. M. H., and Smith, G.: C-band repeat-pass interferometric SAR observations of the forest, IEEE Trans. Geosci. Remote Sens., 35, 25–35, https://doi.org/10.1109/36.551931, 1997.

Avitabile, V.: Carbon stocks of vegetation in the Vu Gia Thu Bon river basin, central Vietnam, Jena, 2014.

Avitabile, V., Baccini, A., Friedl, M. A., and Schmullius, C.: Capabilities and limitations of Landsat and land cover data for aboveground woody biomass estimation of Uganda, Remote Sens. Environ., 117, 366–380, https://doi.org/10.1016/j.rse.2011.10.012, 2012.

Avitabile, V., Herold, M., Heuvelink, G. B. M., Lewis, S. L., Phillips, O. L., Asner, G. P., Armston, J., Ashton, P. S., Banin, L., Bayol, N., Berry, N. J., Boeckx, P., de Jong, B. H. J., DeVries, B., Girardin, C. A. J., Kearsley, E., Lindsell, J. A., Lopez-Gonzalez, G., Lucas, R., Malhi, Y., Morel, A., Mitchard, E. T. A., Nagy, L., Qie, L., Quinones, M. J., Ryan, C. M., Ferry, S. J. W., Sunderland, T., Laurin, G. V., Gatti, R. C., Valentini, R., Verbeeck, H., Wijaya, A., and Willcock, S.: An integrated pan-tropical biomass map using multiple reference datasets, Glob. Change Biol., 22, 1406–1420, https://doi.org/10.1111/gcb.13139, 2016a.

Avitabile, V., Schultz, M., Herold, N., de Bruin, S., Pratihast, A. K., Manh, C. P., Quang, H. V., and Herold, M.: Carbon emissions from land cover change in Central Vietnam, Carbon Manag., 7, 333–346, https://doi.org/10.1080/17583004.2016.1254009, 2016b.

Baccini, A., Goetz, S. J., Walker, W. S., Laporte, N. T., Sun, M., Sulla-Menashe, D., Hackler, J., Beck, P. S. A., Dubayah, R., Friedl, M. A., Samanta, S., and Houghton, R. A.: Estimated carbon dioxide emissions from tropical deforestation improved by carbon-density maps, Nat. Clim. Change, 2, 182–185, https://doi.org/10.1038/nclimate1354, 2012.

Batjes, N., Dijkshoorn, K., van Engelen, V., Fischer, G., Jones, A., Montanarella, L., Petri, M., Prieler, S., Teixeira, E., and Shi, X.: Harmonized World Soil Database, FAO, Rome, Italy and IIASA, Laxenburg, Austria, n.d.

Bispo, P. C., Santos, J. R., Valeriano, M. M., Touzi, R., and Seifert, F. M.: Integration of polarimetric PALSAR attributes and local geomorphometric variables derived from SRTM for forest biomass modeling in central Amazonia, Can. J. Remote Sens., 40, 26–42, https://doi.org/10.1080/07038992.2014.913477, 2014.

Blackard, J., Finco, M., Helmer, E., Holden, G., Hoppus, M., Jacobs, D., Lister, A., Moisen, G., Nelson, M., and Riemann, R.: Mapping U.S. forest biomass using nationwide forest inventory data and moderate resolution information, Remote Sens. Environ., 112, 1658–1677, https://doi.org/10.1016/j.rse.2007.08.021, 2008.

Breiman, L.: Random Forests, Mach. Learn., 45, 5–32, https://doi.org/10.1023/A:1010933404324, 2001.

Brown, S., Gillespie, A. J. R., and Lugo, A. E.: Biomass estimation methods for tropical forests with applications to forest inventory data, For. Sci., 35, 881–902, 1989.

Brown, S., Goslee, K., Casarim, F., Harris, N. L., and Petrova, S.: Sampling Design and Implementation Plan for Guyana's REDD+ Forest Carbon Monitoring System (FCMS): Version 2. Submitted by Winrock International to the Guyana Forestry Commission, GFC 02/08/2010 Addendum, Guyana Forestry Commission, 2014.

Carreiras, J. M. B., Vasconcelos, M. J., and Lucas, R. M.: Understanding the relationship between aboveground biomass and ALOS PALSAR data in the forests of Guinea-Bissau (West Africa), Remote Sens. Environ., 121, 426–442, https://doi.org/10.1016/j.rse.2012.02.012, 2012.

Carreiras, J. M. B., Melo, J. B., and Vasconcelos, M. J.: Estimating the above-ground biomass in miombo savanna woodlands (Mozambique, East Africa) using L-band synthetic aperture radar data, Remote Sens., 5, 1524–1548, https://doi.org/10.3390/rs5041524, 2013.

Chave, J., Andalo, C., Brown, S., Cairns, M. A., Chambers, J. Q., Eamus, D., Fölster, H., Fromard, F., Higuchi, N., Kira, T., Lescure, J.-P., Nelson, B. W., Ogawa, H., Puig, H., Riéra, B., and Yamakura, T.: Tree allometry and improved estimation of carbon stocks and balance in tropical forests, Oecologia, 145, 87–99, https://doi.org/10.1007/s00442-005-0100-x, 2005.

Chave, J., Coomes, D., Jansen, S., Lewis, S. L., Swenson, N. G., and Zanne, A. E.: Towards a worldwide wood economics spectrum, Ecol. Lett., 12, 351–366, https://doi.org/10.1111/j.1461-0248.2009.01285.x, 2009.

Chave, J., Réjou-Méchain, M., Búrquez, A., Chidumayo, E., Colgan, M. S., Delitti, W. B. C., Duque, A., Eid, T., Fearnside, P. M., Goodman, R. C., Henry, M., Martínez-Yrízar, A., Mugasha, W. A., Muller-Landau, H. C., Mencuccini, M., Nelson, B. W., Ngomanda, A., Nogueira, E. M., Ortiz-Malavassi, E., Pélissier, R., Ploton, P., Ryan, C. M., Saldarriaga, J. G., and

Vieilledent, G.: Improved allometric models to estimate the aboveground biomass of tropical trees, Glob. Change Biol., 20, 3177–3190, https://doi.org/10.1111/gcb.12629, 2014.

Chidumayo, E. N.: Miombo ecology and management: an introduction, IT Publications [u.a.], London, 166 pp., 1997.

Cienciala, E., Apltauer, J., Exnerová, Z., and Tatarinov, F.: Biomass functions applicable to oak trees grown in Central-European forestry, J. For. Sci., 54, 109–120, https://doi.org/10.17221/2906-JFS, 2008.

Da Conceição Bispo, P., De Morisson Valeriano, M., and Dos Santos, J. R.: Effects of the geomorphometric characteristics of the local terrain on floristic composition in the central Brazilian Amazon: Local geomorphometry and floristic composition, Austral Ecol., 37, 491–499, https://doi.org/10.1111/j.1442-9993.2011.02310.x, 2012.

Defourny, P., Bontemps, S., Lamarche, C., Brockmann, C., Kirches, G., Boettcher, M., Santoro, M., Ramoino, F., and Arino, O.: ESA Climate Change Initiative - Land Cover project, Products User Guide, version 2.4, available at http://maps.elie.ucl.ac.be/CCI/viewer/index.php, 2014.

DeVries, B., Avitabile, V., Kooistra, L., and Herold, M.: Monitoring the impact of REDD+ implementation in the Unesco Kafa biosphere reserve, 2012.

Drichi, P.: National biomass study, technical report of 1996-2002, Forestry Department, Ministry of Water, Lands & Environment, Kampala, Uganda, 2003.

Falster, D. S., Duursma, R. A., Ishihara, M. I., Barneche, D. R., FitzJohn, R. G., Vårhammar, A., Aiba, M., Ando, M., Anten, N., Aspinwall, M. J., Baltzer, J. L., Baraloto, C., Battaglia, M., Battles, J. J., Bond-Lamberty, B., van Breugel, M., Camac, J., Claveau, Y., Coll, L., Dannoura, M., Delagrange, S., Domec, J.-C., Fatemi, F., Feng, W., Gargaglione, V., Goto, Y., Hagihara, A., Hall, J. S., Hamilton, S., Harja, D., Hiura, T., Holdaway, R., Hutley, L. S., Ichie, T., Jokela, E. J., Kantola, A., Kelly, J. W. G., Kenzo, T., King, D., Kloeppel, B. D., Kohyama, T., Komiyama, A., Laclau, J.-P., Lusk, C. H., Maguire, D. A., le Maire, G., Mäkelä, A., Markesteijn, L., Marshall, J., McCulloh, K., Miyata, I., Mokany, K., Mori, S., Myster, R. W., Nagano, M., Naidu, S. L., Nouvellon, Y., O'Grady, A. P., O'Hara, K. L., Ohtsuka, T., Osada, N., Osunkoya, O. O., Peri, P. L., Petritan, A. M., Poorter, L., Portsmuth, A., Potvin, C., Ransijn, J., Reid, D., Ribeiro, S. C., Roberts, S. D., Rodríguez, R., Saldaña-Acosta, A., Santa-Regina, I., Sasa, K., Selaya, N. G., Sillett, S. C., Sterck, F., Takagi, K., Tange, T., Tanouchi, H., Tissue, D., Umehara, T., Utsugi, H., Vadeboncoeur, M. A., Valladares, F., Vanninen, P., Wang, J. R., Wenk, E., Williams, R., de Aquino Ximenes, F., Yamaba, A., Yamada, T., Yamakura, T., Yanai, R. D., and York, R. A.: BAAD: a Biomass And Allometry Database for woody plants, Ecology, 96, 1445–1445, https://doi.org/10.1890/14-1889.1, 2015.

FAO: FRA 2000 - Global ecological zoning for the Global Forest Resources Assessment 2000, Rome, 2001.

Fick, S. E. and Hijmans, R. J.: Worldclim 2: New 1-km spatial resolution climate surfaces for global land areas, Int. J. Climatol., 37, 4302–4315, https://doi.org/10.1002/joc.5086, 2017.

Forest Management Bureau: Annual Accomplishment Report, 2010.

Gillis, M. D., Omule, A. Y., and Brierley, T.: Monitoring Canada's forests: The National Forest Inventory, For. Chron., 81, 214–221, https://doi.org/10.5558/tfc81214-2, 2005.

Goodman, R. C., Phillips, O. L., del Castillo Torres, D., Freitas, L., Cortese, S. T., Monteagudo, A., and Baker, T. R.: Amazon palm biomass and allometry, For. Ecol. Manag., 310, 994–1004, https://doi.org/10.1016/j.foreco.2013.09.045, 2013.

Goodman, R. C., Phillips, O. L., and Baker, T. R.: The importance of crown dimensions to improve tropical tree biomass estimates, Ecol. Appl., 24, 680–698, https://doi.org/10.1890/13-0070.1, 2014.

Goodman, R. C., Harman Aramburu, M., Gopalakrishna, T., Putz, F. E., Gutiérrez, N., Mena Alvarez, J. L., Aguilar-Amuchastegui, N., and Ellis, P. W.: Carbon emissions and potential emissions reductions from low-intensity selective logging in southwestern Amazonia, For. Ecol. Manag., 439, 18–27, https://doi.org/10.1016/j.foreco.2019.02.037, 2019.

Hansen, M. C., Potapov, P. V., Moore, R., Hancher, M., Turubanova, S. A., Tyukavina, A., Thau, D., Stehman, S. V., Goetz, S. J., Loveland, T. R., Kommareddy, A., Egorov, A., Chini, L., Justice, C. O., and Townshend, J. R. G.: High-resolution global maps of 21-st century forest cover change, Science, 342, 850–853, https://doi.org/10.1126/science.1244693, 2013.

Hu, T., Su, Y., Xue, B., Liu, J., Zhao, X., Fang, J., and Guo, Q.: Mapping global forest aboveground biomass with spaceborne LiDAR, optical imagery, and forest inventory data, Remote Sens., 8, 565, https://doi.org/10.3390/rs8070565, 2016.

Huete, A., Didan, K., Miura, T., Rodriguez, E. P., Gao, X., and Ferreira, L. G.: Overview of the radiometric and biophysical performance of the MODIS vegetation indices, Remote Sens. Environ., 83, 195–213, https://doi.org/10.1016/S0034-4257(02)00096-2, 2002.

INFOR: Informe Final - Inventario continuo de bosques nativos y actualizacion de plantaciones forestales, 2015.

IPCC: IPCC Guidelines for National Greenhouse Gas Inventories, edited by: Eggleston, H. S., Buendia, L., Miwa, K., Ngara, T., and Tanabe, K., Institute for Global Environmental Strategies, Japan, 2006.

de Jong, B. H.: Spatial distribution of biomass and links to reported disturbances in tropical lowland forests of southern Mexico, Carbon Manag., 4, 601–615, https://doi.org/10.4155/cmt.13.60, 2013.

Jung, M. and Zscheischler, J.: A Guided Hybrid Genetic Algorithm for Feature Selection with Expensive Cost Functions, Procedia Comput. Sci., 18, 2337–2346, https://doi.org/10.1016/j.procs.2013.05.405, 2013.

Kattge, J., Díaz, S., Lavorel, S., Prentice, I. C., Leadley, P., Bönisch, G., Garnier, E., Westoby, M., Reich, P. B., Wright, I. J., Cornelissen, J. H. C., Violle, C., Harrison, S. P., Van BODEGOM, P. M., Reichstein, M., Enquist, B. J., Soudzilovskaia, N. A., Ackerly, D. D., Anand, M., Atkin, O., Bahn, M., Baker, T. R., Baldocchi, D., Bekker, R., Blanco, C. C., Blonder, B., Bond, W. J., Bradstock, R., Bunker, D. E., Casanoves, F., Cavender-Bares, J., Chambers, J. Q., Chapin Iii, F. S., Chave, J., Coomes, D., Cornwell, W. K., Craine, J. M., Dobrin, B. H., Duarte, L., Durka, W., Elser, J., Esser, G., Estiarte, M., Fagan, W. F., Fang, J., Fernández-Méndez, F., Fidelis, A., Finegan, B., Flores, O., Ford, H., Frank, D., Freschet, G. T., Fyllas, N. M., Gallagher, R. V., Green, W. A., Gutierrez, A. G., Hickler, T., Higgins, S. I., Hodgson, J. G., Jalili, A., Jansen, S., Joly, C. A., Kerkhoff, A. J., Kirkup, D., Kitajima, K., Kleyer, M., Klotz, S., Knops, J. M. H., Kramer, K., Kühn, I., Kurokawa, H., Laughlin, D., Lee, T. D., Leishman, M., Lens, F., Lenz, T., Lewis, S. L., Lloyd, J., Llusià, J., Louault, F., Ma, S., Mahecha, M. D., Manning, P., Massad, T., Medlyn, B. E., Messier, J., Moles, A. T., Müller, S. C., Nadrowski, K., Naeem, S., Niinemets, Ü., Nöllert, S., Nüske, A., Ogaya, R., Oleksyn, J., Onipchenko, V. G., Onoda, Y., Ordoñez, J., Overbeck, G., et al.: TRY - a global database of plant traits, Glob. Change Biol., 17, 2905–2935, https://doi.org/10.1111/j.1365-2486.2011.02451.x, 2011.

Kearsley, E., de Haulleville, T., Hufkens, K., Kidimbu, A., Toirambe, B., Baert, G., Huygens, D., Kebede, Y., Defourny, P., Bogaert, J., Beeckman, H., Steppe, K., Boeckx, P., and Verbeeck, H.: Conventional tree height–diameter relationships significantly overestimate aboveground carbon stocks in the Central Congo Basin, Nat. Commun., 4, 2269, https://doi.org/10.1038/ncomms3269, 2013.

NACP Aboveground Biomass and Carbon Baseline Data (NBCD 2000): Available on-line at http://daac.ornl.gov from ORNL DAAC, Oak Ridge, Tennessee, U.S.A. http://dx.doi.org/10.3334/ORNLDAAC/1081.

KFS: Statistical yearbook of forestry, Seoul, 2010.

Kindermann, G. E., McCallum, I., Fritz, S., and Obersteiner, M.: A global forest growing stock, biomass and carbon map based on FAO statistics, Silva Fenn., 42, 387–396, https://doi.org/10.14214/sf.244, 2008.

Kitahara, F., Mizoue, N., and Yoshida, S.: Evaluation of data quality in Japanese National Forest Inventory, Environ. Monit. Assess., 159, 331–340, https://doi.org/10.1007/s10661-008-0632-8, 2009.

Komiyama, A., Ong, J. E., and Poungparn, S.: Allometry, biomass, and productivity of mangrove forests: A review, Aquat. Bot., 89, 128–137, https://doi.org/10.1016/j.aquabot.2007.12.006, 2008.

Kottek, M., Grieser, J., Beck, C., Rudolf, B., and Rubel, F.: World map of the Köppen-Geiger climate classification updated, Meteorol. Z., 15, 259–263, https://doi.org/10.1127/0941-2948/2006/0130, 2006.

Liang, J., Zhou, M., Tobin, P. C., McGuire, A. D., and Reich, P. B.: Biodiversity influences plant productivity through niche–efficiency, Proc. Natl. Acad. Sci., 112, 5738–5743, https://doi.org/10.1073/pnas.1409853112, 2015.

Lindsell, J. A. and Klop, E.: Spatial and temporal variation of carbon stocks in a lowland tropical forest in West Africa, For. Ecol. Manag., 289, 10–17, https://doi.org/10.1016/j.foreco.2012.09.045, 2013.

Liu, Y. Y., van Dijk, A. I. J. M., de Jeu, R. A. M., Canadell, J. G., McCabe, M. F., Evans, J. P., and Wang, G.: Recent reversal in loss of global terrestrial biomass, Nat. Clim. Change, 5, 470–474, https://doi.org/10.1038/nclimate2581, 2015.

Marzoli, A.: Inventârio florestal nacional, Maputo, 2007.

Forest Inventory EVALIDator web-application version 1.6.0.00: http://apps.fs.fed.us/Evalidator/evalidator.jsp.

Ministry of Natural Resources and Tourism: National Forest Resources Monitoring and Assessment of Tanzania Mainland - Main Results, 2015.

Mitchard, E. T. A., Saatchi, S. S., Woodhouse, I. H., Nangendo, G., Ribeiro, N. S., Williams, M., Ryan, C. M., Lewis, S. L., Feldpausch, T. R., and Meir, P.: Using satellite radar backscatter to predict above-ground woody biomass: A consistent

relationship across four different African landscapes, Geophys. Res. Lett., 36, 1–6, https://doi.org/10.1029/2009GL040692, 2009.

Mitchard, E. T. A., Saatchi, S. S., Lewis, S. L., Feldpausch, T. R., Woodhouse, I. H., Sonké, B., Rowland, C., and Meir, P.: Measuring biomass changes due to woody encroachment and deforestation/degradation in a forest savanna boundary region of central Africa using multi-temporal L-band radar backscatter, Remote Sens. Environ., 115, 2861–2873, 2011.

Morel, A. C., Saatchi, S. S., Malhi, Y., Berry, N. J., Banin, L., Burslem, D., Nilus, R., and Ong, R. C.: Estimating aboveground biomass in forest and oil palm plantation in Sabah, Malaysian Borneo using ALOS PALSAR data, For. Ecol. Manag., 262, 1786–1798, https://doi.org/10.1016/j.foreco.2011.07.008, 2011.

Moreno-Martínez, Á., Camps-Valls, G., Kattge, J., Robinson, N., Reichstein, M., van Bodegom, P., Kramer, K., Cornelissen, J. H. C., Reich, P., Bahn, M., Niinemets, Ü., Peñuelas, J., Craine, J. M., Cerabolini, B. E. L., Minden, V., Laughlin, D. C., Sack, L., Allred, B., Baraloto, C., Byun, C., Soudzilovskaia, N. A., and Running, S. W.: A methodology to derive global maps of leaf traits using remote sensing and climate data, Remote Sens. Environ., 218, 69–88, https://doi.org/10.1016/j.rse.2018.09.006, 2018.

Muchiri, M. and Muga, M.: A preliminary yield model for natural Yushania alpina Bamboo in Kenya, J. Nat. Sci. Res., 3, 77–84, 2013.

Murdiyarso, D., Donato, D., Kauffman, J. B., Kurnianto, S., Stidham, M., and Kanninen, M.: Carbon storage in mangrove and peatland ecosystems: a preliminary account from plots in Indonesia, Bogor, Indonesia, 2010.

Myneni, R. B., Hoffman, S., Knyazikhin, Y., Privette, J. L., Glassy, J., Tian, Y., Wang, Y., Song, X., Zhang, Y., Smith, G. R., Lotsch, A., Friedl, M., Morisette, J. T., Votava, P., Nemani, R. R., and Running, S. W.: Global products of vegetation leaf area and fraction absorbed PAR from year one of MODIS data, Remote Sens. Environ., 83, 214–231, https://doi.org/10.1016/S0034-4257(02)00074-3, 2002.

Pan, Y., Birdsey, R. A., Fang, J., Houghton, R., Kauppi, P. E., Kurz, W. A., Phillips, O. L., Shvidenko, A., Lewis, S. L., Canadell, J. G., Ciais, P., Jackson, R. B., Pacala, S. W., McGuire, A. D., Piao, S., Rautiainen, A., Sitch, S., and Hayes, D.: A large and persistent carbon sink in the world's forests, Science, 333, 988–993, https://doi.org/10.1126/science.1201609, 2011.

Paul, K. I., Roxburgh, S. H., Chave, J., England, J. R., Zerihun, A., Specht, A., Lewis, T., Bennett, L. T., Baker, T. G., Adams, M. A., Huxtable, D., Montagu, K. D., Falster, D. S., Feller, M., Sochacki, S., Ritson, P., Bastin, G., Bartle, J., Wildy, D., Hobbs, T., Larmour, J., Waterworth, R., Stewart, H. T. L., Jonson, J., Forrester, D. I., Applegate, G., Mendham, D., Bradford, M., O'Grady, A., Green, D., Sudmeyer, R., Rance, S. J., Turner, J., Barton, C., Wenk, E. H., Grove, T., Attiwill, P. M., Pinkard, E., Butler, D., Brooksbank, K., Spencer, B., Snowdon, P., O'Brien, N., Battaglia, M., Cameron, D. M., Hamilton, S., Mcauthur, G., and Sinclair, J.: Testing the generality of above-ground biomass allometry across plant functional types at the continent scale, Glob. Change Biol., 22, 2106–2124, https://doi.org/10.1111/gcb.13201, 2016.

Pearson, T. R. H., Brown, S. L., and Birdsey, R. A.: Measurement guidelines for the sequestration of forest carbon, U.S. Department of Agriculture, Forest Service, Northern Research Station, Newtown Square, PA, https://doi.org/10.2737/NRS-GTR-18, 2007.

Phillips, O. L., Vásquez Martínez, R., Núñez Vargas, P., Lorenzo Monteagudo, A., Chuspe Zans, M.-E., Galiano Sánchez, W., Peña Cruz, A., Timaná, M., Yli-Halla, M., and Rose, S.: Efficient plot-based floristic assessment of tropical forests, J. Trop. Ecol., 19, 629–645, https://doi.org/10.1017/S0266467403006035, 2003.

Pinzon, J. and Tucker, C.: A Non-Stationary 1981–2012 AVHRR NDVI3g Time Series, Remote Sens., 6, 6929–6960, https://doi.org/10.3390/rs6086929, 2014.

Pirotti, F., Laurin, G., Vettore, A., Masiero, A., and Valentini, R.: Small Footprint Full-Waveform Metrics Contribution to the Prediction of Biomass in Tropical Forests, Remote Sens., 6, 9576–9599, https://doi.org/10.3390/rs6109576, 2014.

DUE GlobBiomass - Algorithm Theoretical Basis Document: http://globbiomass.org/products/global-mapping/.

Rodríguez-Veiga, P., Quegan, S., Carreiras, J., Persson, H. J., Fransson, J. E. S., Hoscilo, A., Ziółkowski, D., Stereńczak, K., Lohberger, S., Stängel, M., Berninger, A., Siegert, F., Avitabile, V., Herold, M., Mermoz, S., Bouvet, A., Le Toan, T., Carvalhais, N., Santoro, M., Cartus, O., Rauste, Y., Mathieu, R., Asner, G. P., Thiel, C., Pathe, C., Schmullius, C., Seifert, F. M., Tansey, K., and Balzter, H.: Forest biomass retrieval approaches from Earth Observation in different biomes, Int. J. Appl. Earth Obs. Geoinformation, 77, 53–68, https://doi.org/10.1016/j.jag.2018.12.008, 2019.

Ryan, C. M., Williams, M., and Grace, J.: Above- and belowground carbon stocks in a miombo woodland landscape of Mozambique, Biotropica, 43, 423–432, https://doi.org/10.1111/j.1744-7429.2010.00713.x, 2011.

Ryan, C. M., Hill, T., Woollen, E., Ghee, C., Mitchard, E., Cassells, G., Grace, J., Woodhouse, I. H., and Williams, M.: Quantifying small-scale deforestation and forest degradation in African woodlands using radar imagery, Glob. Change Biol., 18, 243–257, https://doi.org/10.1111/j.1365-2486.2011.02551.x, 2012.

Saatchi, S. S., Harris, N. L., Brown, S., Lefsky, M., Mitchard, E. T. A., Salas, W., Zutta, B. R., Buermann, W., Lewis, S. L., Hagen, S., Petrova, S., White, L., Silman, M., and Morel, A.: Benchmark map of forest carbon stocks in tropical regions across three continents, Proc. Natl. Acad. Sci., 108, 9899–9904, https://doi.org/10.1073/pnas.1019576108, 2011.

Santoro, M., Beer, C., Cartus, O., Schmullius, C., Shvidenko, A., McCallum, I., Wegmüller, U., and Wiesmann, A.: Retrieval of growing stock volume in boreal forest using hyper-temporal series of Envisat ASAR ScanSAR backscatter measurements, Remote Sens. Environ., 115, 490–507, https://doi.org/10.1016/j.rse.2010.09.018, 2011.

Santoro, M., Beaudoin, A., Beer, C., Cartus, O., Fransson, J. E. S., Hall, R. J., Pathe, C., Schepaschenko, D., Schmullius, C., Shvidenko, A., Thurner, M., and Wegmüller, U.: Forest growing stock volume of the northern hemisphere: Spatially explicit estimates for 2010 derived from Envisat ASAR data, Remote Sens. Environ., 168, 316–334, https://doi.org/10.1016/j.rse.2015.07.005, 2015.

dos-Santos, M. N., Keller, M. M., and Morton, D. C.: Carbon Monitoring System (CMS)LiDAR Surveys over Selected Forest Research Sites, Brazilian Amazon, 2008-2018, 128587.53907999989 MB, https://doi.org/10.3334/ORNLDAAC/1644, 2019.

Schelhaas, M. J., Clerkx, A. P. P. M., Daamen, W. P., Oldenburger, J. F., Velema, G., Schnitger, P., Schoonderwoerd, H., and Kramer, H.: Zesde Nederlandse Bosinventarisatie; Methoden en basisresultaten, Wageningen, Alterra Wageningen UR (University & Research Centre)., 2014.

Schepaschenko, D., Shvidenko, A., Usoltsev, V., Lakyda, P., Luo, Y., Vasylyshyn, R., Lakyda, I., Myklush, Y., See, L., McCallum, I., Fritz, S., Kraxner, F., and Obersteiner, M.: A dataset of forest biomass structure for Eurasia, Sci. Data, 4, 1–11, https://doi.org/10.1038/sdata.2017.70, 2017.

Schepaschenko, D., Chave, J., Phillips, O. L., Lewis, S. L., Davies, S. J., Réjou-Méchain, M., Sist, P., Scipal, K., Perger, C., Herault, B., Labrière, N., Hofhansl, F., Affum-Baffoe, K., Aleinikov, A., Alonso, A., Amani, C., Araujo-Murakami, A., Armston, J., Arroyo, L., Ascarrunz, N., Azevedo, C., Baker, T., Bałazy, R., Bedeau, C., Berry, N., Bilous, A. M., Bilous, S. Yu., Bissiengou, P., Blanc, L., Bobkova, K. S., Braslavskaya, T., Brienen, R., Burslem, D. F. R. P., Condit, R., Cuni-Sanchez, A., Danilina, D., del Castillo Torres, D., Derroire, G., Descroix, L., Sotta, E. D., d'Oliveira, M. V. N., Dresel, C., Erwin, T., Evdokimenko, M. D., Falck, J., Feldpausch, T. R., Foli, E. G., Foster, R., Fritz, S., Garcia-Abril, A. D., Gornov, A., Gornova, M., Gothard-Bassébé, E., Gourlet-Fleury, S., Guedes, M., Hamer, K. C., Susanty, F. H., Higuchi, N., Coronado, E. N. H., Hubau, W., Hubbell, S., Ilstedt, U., Ivanov, V. V., Kanashiro, M., Karlsson, A., Karminov, V. N., Killeen, T., Koffi, J.-C. K., Konovalova, M., Kraxner, F., Krejza, J., Krisnawati, H., Krivobokov, L. V., Kuznetsov, M. A., Lakyda, I., Lakyda, P. I., Licona, J. C., Lucas, R. M., Lukina, N., Lussetti, D., Malhi, Y., Manzanera, J. A., Marimon, B., Junior, B. H. M., Martinez, R. V., Martynenko, O. V., Matsala, M., Matyashuk, R. K., Mazzei, L., Memiaghe, H., Mendoza, C., Mendoza, A. M., Moroziuk, O. V., Mukhortova, L., Musa, S., Nazimova, D. I., Okuda, T., Oliveira, L. C., Ontikov, P. V., et al.: The Forest Observation System, building a global reference dataset for remote sensing of forest biomass, Sci. Data, 6, 198, https://doi.org/10.1038/s41597-019-0196-1, 2019.

Schepaschenko, D. G., Shvidenko, A. Z., Lesiv, M. Yu., Ontikov, P. V., Shchepashchenko, M. V., and Kraxner, F.: Estimation of forest area and its dynamics in Russia based on synthesis of remote sensing products, Contemp. Probl. Ecol., 8, 811–817, https://doi.org/10.1134/S1995425515070136, 2015.

Schrodt, F., Kattge, J., Shan, H., Fazayeli, F., Joswig, J., Banerjee, A., Reichstein, M., Bönisch, G., Díaz, S., Dickie, J., Gillison, A., Karpatne, A., Lavorel, S., Leadley, P., Wirth, C. B., Wright, I. J., Wright, S. J., and Reich, P. B.: BHPMF - a hierarchical Bayesian approach to gap-filling and trait prediction for macroecology and functional biogeography: Gap-filling in trait databases, Glob. Ecol. Biogeogr., 24, 1510–1521, https://doi.org/10.1111/geb.12335, 2015.

Sexton, J. O., Song, X. P., Feng, M., Noojipady, P., Anand, A., Huang, C., Kim, D. H., Collins, K. M., Channan, S., DiMiceli, C., and Townshend, J. R.: Global, 30-m resolution continuous fields of tree cover: Landsat-based rescaling of MODIS vegetation continuous fields with lidar-based estimates of error, Int. J. Digit. Earth, 6, 427–448, https://doi.org/10.1080/17538947.2013.786146, 2013.

Simard, M., Pinto, N., Fisher, J. B., and Baccini, A.: Mapping forest canopy height globally with spaceborne LiDAR, J. Geophys. Res., 116, https://doi.org/10.1029/2011JG001708, 2011.

Slik, J. W. F., Paoli, G., McGuire, K., Amaral, I., Barroso, J., Bastian, M., Blanc, L., Bongers, F., Boundja, P., Clark, C., Collins, M., Dauby, G., Ding, Y., Doucet, J.-L., Eler, E., Ferreira, L., Forshed, O., Fredriksson, G., Gillet, J.-F., Harris, D., Leal, M., Laumonier, Y., Malhi, Y., Mansor, A., Martin, E., Miyamoto, K., Araujo-Murakami, A., Nagamasu, H., Nilus, R., Nurtjahya, E., Oliveira, Á., Onrizal, O., Parada-Gutierrez, A., Permana, A., Poorter, L., Poulsen, J., Ramirez-Angulo, H., Reitsma, J., Rovero, F., Rozak, A., Sheil, D., Silva-Espejo, J., Silveira, M., Spironelo, W., ter Steege, H., Stevart, T., Navarro-Aguilar, G. E., Sunderland, T., Suzuki, E., Tang, J., Theilade, I., van der Heijden, G., van Valkenburg, J., Van Do,

T., Vilanova, E., Vos, V., Wich, S., Wöll, H., Yoneda, T., Zang, R., Zhang, M.-G., and Zweifel, N.: Large trees drive forest aboveground biomass variation in moist lowland forests across the tropics: Large trees and tropical forest biomass, Glob. Ecol. Biogeogr., 22, 1261–1271, https://doi.org/10.1111/geb.12092, 2013.

Tabacchi, G., Di Cosmo, L., and Gasparini, P.: Aboveground tree volume and phytomass prediction equations for forest species in Italy, Eur. J. For. Res., 130, 911–934, https://doi.org/10.1007/s10342-011-0481-9, 2011.

TERN AusCover: Biomass Plot Library - National collation of tree and shrub inventory data, allometric model predictions of above and below-ground biomass, Australia, 2016.

Thurner, M., Beer, C., Santoro, M., Carvalhais, N., Wutzler, T., Schepaschenko, D., Shvidenko, A., Kompter, E., Ahrens, B., Levick, S. R., and Schmullius, C.: Carbon stock and density of northern boreal and temperate forests, Glob. Ecol. Biogeogr., 23, 297–310, https://doi.org/10.1111/geb.12125, 2014.

Tramontana, G., Jung, M., Schwalm, C. R., Ichii, K., Camps-Valls, G., Ráduly, B., Reichstein, M., Arain, M. A., Cescatti, A., Kiely, G., Merbold, L., Serrano-Ortiz, P., Sickert, S., Wolf, S., and Papale, D.: Predicting carbon dioxide and energy fluxes across global FLUXNET sites with regression algorithms, Biogeosciences, 13, 4291–4313, https://doi.org/10.5194/bg-13-4291-2016, 2016.

Ung, C.-H., Bernier, P., and Guo, X.-J.: Canadian national biomass equations: new parameter estimates that include British Columbia data, Can. J. For. Res., 38, 1123–1132, https://doi.org/10.1139/X07-224, 2008.

Urquiza-Haas, T., Dolman, P. M., and Peres, C. A.: Regional scale variation in forest structure and biomass in the Yucatan Peninsula, Mexico: Effects of forest disturbance, For. Ecol. Manag., 247, 80–90, https://doi.org/10.1016/j.foreco.2007.04.015, 2007.

Vaglio Laurin, G., Chen, Q., Lindsell, J. A., Coomes, D. A., Frate, F. D., Guerriero, L., Pirotti, F., and Valentini, R.: Above ground biomass estimation in an African tropical forest with lidar and hyperspectral data, ISPRS J. Photogramm. Remote Sens., 89, 49–58, https://doi.org/10.1016/j.isprsjprs.2014.01.001, 2014.

Vieilledent, G., Gardi, O., Grinand, C., Burren, C., Andriamanjato, M., Camara, C., Gardner, C. J., Glass, L., Rasolohery, A., Rakoto Ratsimba, H., Gond, V., and Rakotoarijaona, J.-R.: Bioclimatic envelope models predict a decrease in tropical forest carbon stocks with climate change in Madagascar, J. Ecol., 104, 703–715, https://doi.org/10.1111/1365-2745.12548, 2016.

Wijaya, A., Liesenberg, V., Susanti, A., Karyanto, O., and Verchot, L. V.: Estimation of Biomass Carbon Stocks over Peat Swamp Forests using Multi-Temporal and Multi-Polratizations SAR Data, ISPRS - Int. Arch. Photogramm. Remote Sens. Spat. Inf. Sci., XL-7/W3, 551–556, https://doi.org/10.5194/isprsarchives-XL-7-W3-551-2015, 2015.

Willcock, S., Phillips, O. L., Platts, P. J., Balmford, A., Burgess, N. D., Lovett, J. C., Ahrends, A., Bayliss, J., Doggart, N., Doody, K., Fanning, E., Green, J. M., Hall, J., Howell, K. L., Marchant, R., Marshall, A. R., Mbilinyi, B., Munishi, P. K., Owen, N., Swetnam, R. D., Topp-Jorgensen, E. J., and Lewis, S. L.: Quantifying and understanding carbon storage and sequestration within the Eastern Arc Mountains of Tanzania, a tropical biodiversity hotspot, Carbon Balance Manag., 9, 2, https://doi.org/10.1186/1750-0680-9-2, 2014.

Wilson, A. M. and Jetz, W.: Remotely Sensed High-Resolution Global Cloud Dynamics for Predicting Ecosystem and Biodiversity Distributions, PLOS Biol., 14, e1002415, https://doi.org/10.1371/journal.pbio.1002415, 2016.

WWF and ÖBf: Xe Pian REDD+ project document, Gland, Switzerland, 2013.

Yarie, J., Kane, E. S., and Mack, M. C.: Aboveground Biomass Equations for the Trees of Interior Alaska, Bulletin, 115, 2007.

Zhang, R., Zhou, X., Ouyang, Z., Avitabile, V., Qi, J., Chen, J., and Giannico, V.: Estimating aboveground biomass in subtropical forests of China by integrating multisource remote sensing and ground data, Remote Sens. Environ., 232, 111341, https://doi.org/10.1016/j.rse.2019.111341, 2019.

Zhu, L.: China Forestry Statistical Yearbook 2009, edited by: Administration, S. F., China Forestry PressZhu, L., 498 pp., 2010.